Spectral induced polarization of Na-montmorillonite dispersions

Philippe Leroy, Maximilian Weigand, Guillaume Mériguet, Egon Zimmermann, Christophe Tournassat, Fritjof Fagerlund, Andreas Kemna, Johan Alexander Huisman

▶ **To cite this version:**

Philippe Leroy, Maximilian Weigand, Guillaume Mériguet, Egon Zimmermann, Christophe Tournassat, et al.. Spectral induced polarization of Na-montmorillonite dispersions. Journal of Colloid and Interface Science, 2017, 505, pp.1093-1110. 10.1016/j.jcis.2017.06.071 . insu-01546901

HAL Id: insu-01546901
https://insu.hal.science/insu-01546901

Submitted on 26 Jun 2017

HAL is a multi-disciplinary open access archive for the deposit and dissemination of scientific research documents, whether they are published or not. The documents may come from teaching and research institutions in France or abroad, or from public or private research centers.

L'archive ouverte pluridisciplinaire **HAL**, est destinée au dépôt et à la diffusion de documents scientifiques de niveau recherche, publiés ou non, émanant des établissements d'enseignement et de recherche français ou étrangers, des laboratoires publics ou privés.

Distributed under a Creative Commons Attribution - NonCommercial - NoDerivatives 4.0 International License

Accepted Manuscript

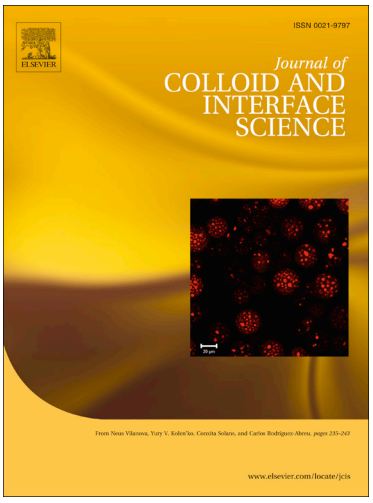

Regular Article

Spectral induced polarization of Na-montmorillonite dispersions

Philippe Leroy, Maximilian Weigand, Guillaume Mériguet, Egon Zimmermann, Christophe Tournassat, Fritjof Fagerlund, Andreas Kemna, Johan Alexander Huisman

PII: S0021-9797(17)30727-0
DOI: http://dx.doi.org/10.1016/j.jcis.2017.06.071
Reference: YJCIS 22498

To appear in: *Journal of Colloid and Interface Science*

Received Date: 18 March 2017
Revised Date: 27 May 2017
Accepted Date: 20 June 2017

Please cite this article as: P. Leroy, M. Weigand, G. Mériguet, E. Zimmermann, C. Tournassat, F. Fagerlund, A. Kemna, J. Alexander Huisman, Spectral induced polarization of Na-montmorillonite dispersions, *Journal of Colloid and Interface Science* (2017), doi: http://dx.doi.org/10.1016/j.jcis.2017.06.071

This is a PDF file of an unedited manuscript that has been accepted for publication. As a service to our customers we are providing this early version of the manuscript. The manuscript will undergo copyediting, typesetting, and review of the resulting proof before it is published in its final form. Please note that during the production process errors may be discovered which could affect the content, and all legal disclaimers that apply to the journal pertain.

ACCEPTED MANUSCRIPT

Spectral induced polarization of Na-montmorillonite dispersions

Philippe Leroy[1,2*], Maximilian Weigand[3], Guillaume Mériguet[4], Egon Zimmermann[5], Christophe Tournassat[6], Fritjof Fagerlund[2], Andreas Kemna[3], Johan Alexander Huisman[7]

[1] BRGM, French Geological Survey, 45060 Orléans, France.

[2] Department of Earth Sciences, Uppsala University, 75236 Uppsala, Sweden.

[3] Department of Geophysics, Steinmann Institute, Bonn University, 53115 Bonn, Germany.

[4] PHENIX, Pierre and Marie Curie University - CNRS, UMR 8234, 75252 Paris, France.

[5] Electronic Systems, ZEA 2, Central Institute of Engineering, Electronics and Analytics, Forschungszentrum Jülich, 52425 Jülich, Germany.

[6] Université d'Orléans - CNRS/INSU - BRGM, UMR 7327 Institut des Sciences de la Terre d'Orléans, 45071 Orléans, France.

[7] Agrosphere institute, IBG 3, Institute for Bio- and Geosciences, Forschungszentrum Jülich, 52425 Jülich, Germany.

[*]Corresponding author and mailing address:

Philippe Leroy

BRGM

3 Avenue Claude Guillemin

45060 Orléans Cedex 2, France

E-mail: p.leroy@brgm.fr

Tel: +33 (0)2 38 64 39 73

Intended for publication in Journal of Colloid and Interface Science

ACCEPTED MANUSCRIPT

Abstract

Montmorillonite (Mt) clays have a high specific surface area and surface charge, which confer them remarkable adsorption properties. Nevertheless, their electrochemical and aggregation behavior are not completely elucidated because of the complexity of their microstructural and interfacial properties. In this work, the conductive and dispersive properties of Na-Mt suspensions of weight fractions 0.5 to 5.2% were investigated for the first time using the spectral induced polarization method. A four-electrode system was used to reduce errors introduced by electrode polarization and contact resistances. Complex conductivity spectra in the low-frequency range of 0.1 Hz to 45 kHz were successfully described using a triple layer model of the basal surface of Mt and a complex conductivity model that considers conduction of the diffuse layer and polarization of the Stern layer. Aggregate size distributions were inferred from inverted relaxation time distributions. We found that the negative and permanent surface charge of the basal plane of Na-Mt controls its quadrature (imaginary) conductivity, which is not very sensitive to pH and salinity (NaCl) in the 100 Hz to 45 kHz frequency range. For lower frequencies, the sudden increase of the quadrature conductivity at the highest salinities was explained by considering coagulation of Na-Mt particles.

Keywords: Na-montmorillonite, dispersions, spectral induced polarization, conductivity, dielectric permittivity, basal plane, surface charge, Stern layer, diffuse layer.

ACCEPTED MANUSCRIPT

1. Introduction

Clay minerals are abundant in regolith and sedimentary rocks [1, 2]. Understanding the electrochemical properties of clays is relevant in environmental geoscience, geotechnics, geothermy, and gas and petroleum exploration [3-7]. Among clays, montmorillonite (Mt) is an important subgroup of smectite [8, 9]. It is the main component of bentonite, which is used as a backfill material for the storage of domestic waste in landfills and of high-level nuclear waste in geological formations [5, 10].

The microstructural and interfacial properties of Mt in water are complex because it forms aggregates constituted of several interacting Mt particles [11, 12]. These particles are made of a succession of TOT layers containing a central octahedral (O) sheet between two inward-pointing tetrahedral (T) sheets (2:1 clay [8]). Their surface charge distribution is heterogeneous. Isomorphic substitution in the solid induces a negative and permanent surface charge of their basal plane (of value between –0.15 and –0.1 C m^{-2}) and the presence of protonated oxygen atoms at their edge results in a pH and salinity-dependent surface charge [12-14]. Mt particles have a lamellar shape (their thickness is few nm and their length is hundreds of nm) and hence a high specific surface area (several hundreds of m^2 g^{-1}) [10].

Currently, molecular dynamics simulations and surface complexation models may accurately describe the electrochemical properties of the basal plane of Mt particles [14-18]. The electrochemical properties of the edge plane remain partly unknown notably because of the spillover effect of the negative electrostatic potential of the basal surface on the electrostatic potential of the edge surface [13, 19]. The accuracy of the models predictions may decrease significantly when the electrochemical properties of Mt aggregates are investigated because of the interactions between Mt particles [11, 12,

ACCEPTED MANUSCRIPT

14]. Furthermore, the aggregation behavior of Mt particles remains not completely elucidated [20, 21]. For these reasons, there is a need for laboratory measurements such as complex impedance measurements to evaluate the predictions of molecular dynamics simulations and surface complexation models of Mt dispersions in well-controlled chemical conditions.

Mt dispersions exhibit a gigantic dielectric permittivity when they are influenced by a sinusoidal electrical field in the kHz to MHz frequency range [22]. This phenomenon is a manifestation of the polarization of the electric double layer (EDL) (also named alpha-relaxation [23]) that compensates the surface charge of clay particles [23]. The dielectric permittivity of Mt dispersions has been measured for frequencies superior or equal to kHz with a two-electrode system [22, 24-32]. Nevertheless, little is known about their polarization for lower frequencies because of the problem of electrode polarization [33]. The spectral induced polarization (SIP) method uses a four-electrode system to measure the complex impedance in the mHz to kHz frequency range [34-36]. In contrast to the two-electrode system, the current is injected through two electrodes and the two other electrodes measure the resulting voltage. The two current and potential electrodes are appropriately separated to diminish effects of electrode polarization [37].

To the best of our knowledge, no study has used a four-electrode system to measure the induced polarization of Mt dispersions for frequencies below kHz. In this work, we present complex conductivity measurements on Na-Mt dispersions of weight fractions 0.5 to 5.2% in the 0.1 Hz to 45 kHz frequency range. These measurements were inverted to obtain the relaxation time distributions. They were also interpreted using a surface complexation model of the basal surface of Na-Mt combined with a mechanistic

ACCEPTED MANUSCRIPT

SIP model that considers conduction of the diffuse layer and polarization of the Stern layer. In the manuscript, the structural and electrical properties of Mt and the complex conductivity model are first explained. Then, the sample preparation and the experimental set-up are presented. Finally, the measured and computed complex conductivities of Na-Mt dispersions are showed and discussed.

2. Theoretical background on the properties of montmorillonite and complex conductivity model

2.1. Structural and electrical properties of montmorillonite

Montmorillonite is a member of the dioctahedral smectite clay group [8, 9]. Mt dispersions contain Mt aggregates made of very elongated particles that are composed of a succession of TOT layers [16, 38]. Each TOT layer has a negative and permanent surface charge at its basal surface ({001} plane) because of the isomorphic substitutions of Si^{4+} by Al^{3+} and Fe^{3+} ions in the tetrahedral sheets and of Al^{3+} and Fe^{3+} by Mg^{2+} and Fe^{2+} ions in the octahedral sheet. Most of the isomorphic substitutions occur in the octahedral sheet and the negative surface charge is compensated by cations adsorbed in the interlayeyr space, sandwiched between two TOT layers, or on the outer basal surface (Fig. 1). The edge surface contains protonated and deprotonated oxygen atoms and has a surface charge that depends on pH and salinity [10, 13, 19].

ACCEPTED MANUSCRIPT

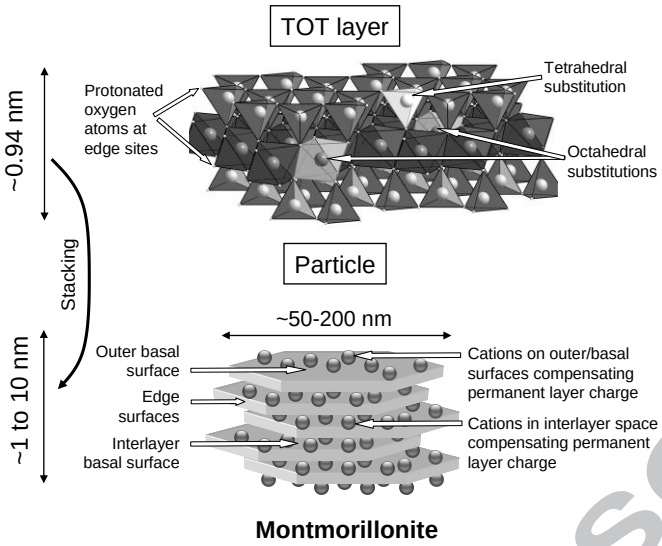

Fig. 1. Sketch of the structure of a montmorillonite TOT layer and particle (from Ref. [16] with the permission of the Publisher).

Each TOT layer is very elongated, ~ 1 nm thick and 50–200 nm long [10] (Fig. 1). The surface area of a TOT layer is thus dominated by the contribution of the basal surface, as the edge surface area only represents a minor part of the total surface area. From crystallographic considerations, it can be estimated that the total specific surface area of a Mt TOT layer is about 780 $m^2\ g^{-1}$ [14], from which the edge surface share is about 10–30 $m^2\ g^{-1}$ and the basal surface share is about 750–770 $m^2\ g^{-1}$ [39, 40]. The specific surface area of the outer basal surface, SS_b^o, is related to the number n_c of TOT layers that are stacked in a single Mt particle (Fig. 1):

$$SS_b^o = \frac{SS_b}{n_c}, \tag{1}$$

where SS_b is the total specific surface area of the basal surface (in $m^2\ g^{-1}$). The number n_c rarely exceeds 10 in water [14]. According to viscosity and light-transmission

ACCEPTED MANUSCRIPT

experiments, Na-Mt dispersions in diluted water (ionic strengths typically $\leq 10^{-3}$ M) contain particles made up of 1–2 TOT layers, whereas Ca-Mt or Mg-Mt dispersions contain particles made up of 6–10 TOT layers [41].

Each Mt particle is surrounded by an EDL that compensates the surface charge not compensated by the counter-ions in the interlayer space [27, 42] (Fig. 2). The EDL of Mt is made of a compact layer containing mostly counter-ions, the Stern layer, and of a diffuse layer containing counter-ions in majority and co-ions [3, 16, 18]. The thickness of the diffuse layer can be considerably larger than the thickness of the Mt particle, e.g., several tens of nanometers in diluted water. The thickness of the diffuse layer decreases significantly (as the inverse of the square root of the ionic strength) when the ionic strength increases because of the compression of the diffuse layer [43, 44]. Ionic interactions in the EDL are dominated by the electrostatic interactions between the external surface of Mt and ions in aqueous solution [43, 45]. Beyond the EDL, there is the neutral water [46].

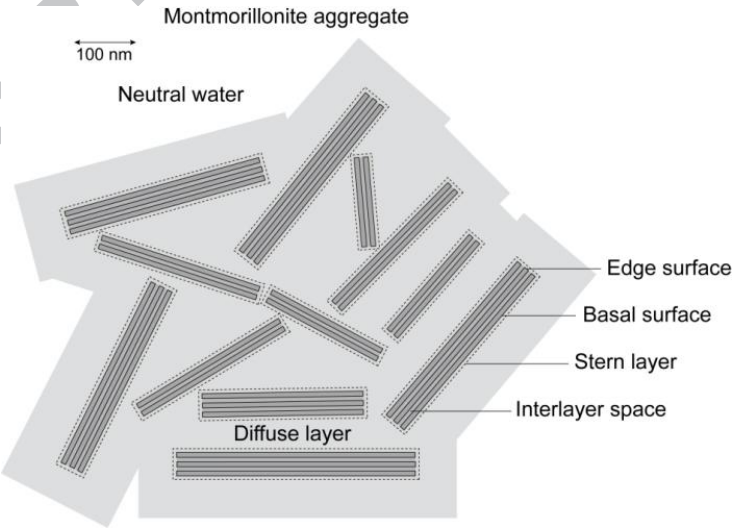

Fig. 2. Sketch of a Mt aggregate containing Mt particles surrounded by their Stern and diffuse layer (the thickness of the particles is larger than in reality, from Ref. [16] with the permission of the Publisher).

ACCEPTED MANUSCRIPT

The dispersion and aggregation of Mt in water are strongly dependent on its surface charge and hence on the water chemical composition [12, 47]. Mt particles can be attracted when their positively charged edge surface interacts with the negatively charged basal surface of another particle ("edge-to-face" interactions favored under acidic conditions [12]). Attractive "Edge-to-edge" interactions may be favored under neutral conditions when the charge of the edge surface is very low because of attractive van der Waals interactions [48]. Repulsive "face-to-face" interactions may be favored under basic conditions because the charge of the edge surface is negative [22]. Even under basic conditions, it has been observed that Na-Mt particles form aggregates in water [26, 28]. This phenomenon can be explained by the presence of a long-range Coulombic attractive force between Na-Mt particles that was not described by the DLVO theory [11]. When the salinity of the aqueous solution reaches the critical coagulation concentration, Mt particles coagulate and form larger and denser Mt aggregates [9, 12, 38].

2.2. Complex conductivity model

The conductivity of Na-Mt dispersions was modeled by considering that Na-Mt particles form aggregates containing both neutral and diffuse layer water. We consider thick diffuse layers, that is, diffuse layers larger than the thickness of a Na-Mt particle, and the effect of electro-osmosis on their electrical conductivity. The diffuse layer is assumed to contribute to the volume conductivity and not to fully polarize because the volume of neutral water controlling the diffuse layer polarization is restricted. We consider that most of the counter-charge is located in the Stern layer and that the Stern

ACCEPTED MANUSCRIPT

layer polarizes. We also neglect the Maxwell-Wagner polarization due to the charge build-up at the boundary between clay and water because of the low solid content of the investigated Na-Mt dispersions (<2% of the total volume) and the low-frequency range of our complex conductivity measurements (Appendix A).

The fraction of the counter-charge in the Stern layer is a parameter of our conductivity model that was directly computed by our surface complexation model. Our conductivity model also depends on the aggregate size distribution (ASD), which was computed by inverting the complex conductivity spectra and assuming a value of the diffusion coefficient of the counter-ions in the Stern layer.

2.2.1. Surface complexation model

The modified triple layer model (TLM) of Leroy et al. [16] was used to compute the electrochemical properties of the Na-Mt particles as a function of the measured cation exchange capacity (CEC) and water chemical composition (Fig. 3). We did not use a surface complexation model for the edge surface of Na-Mt because its surface area (between 10 and 30 m^2 g^{-1} [39, 40]) can be neglected compared to the external surface area of the basal surface (between 375 and 750 m^2 g^{-1} [10, 41]). In addition, no surface complexation model has been developed yet to describe the Stern layer at the edge surface of Na-Mt [19].

ACCEPTED MANUSCRIPT

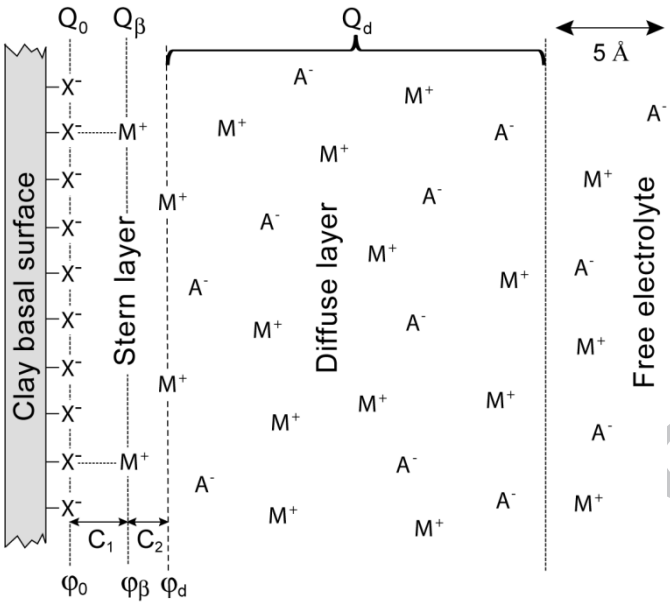

Fig. 3. TLM of the basal surface of Na-Mt in contact with a 1:1 electrolyte (e.g., NaCl). The parameters "φ", "Q" and "C" stand for the electrical potential, the surface charge density, and the capacitance, respectively (from Ref. [16] with the permission of the Publisher).

The TLM of Leroy et al. [16] describes the sorption of Na^+ ion in the Stern layer at the basal surface. It was modified to consider the sorption of H^+ ion [15]. This yields:

$$> X^- + Na^+ \Leftrightarrow > X^- - Na^+, K_{Na}, \quad (2)$$

$$> X^- + H^+ \Leftrightarrow > X^- - H^+, K_H, \quad (3)$$

where $> X^-$ are the negative surface sites (resulting from the isomorphic substitutions in the solid), and K_{Na} and K_H are the equilibrium adsorption constants. In Eq. (3), H^+ ion was assumed to be adsorbed in the Stern layer and not directly on the surface because it may be adsorbed as H_3O^+ ions [49, 50].

By combining Eqs. (2) and (3), we obtained:

ACCEPTED MANUSCRIPT

$$> X^- - Na^+ + H^+ \Leftrightarrow > X^- - H^+ + Na^+ , K_{HNa}, \quad (4)$$

where $K_{HNa} = K_H / K_{Na}$ is the Gaines and Thomas selectivity coefficient describing the exchange of the Na^+ with the H^+ ion (dimensionless, $K_{HNa} = 3.16$ [19] and $K_{Na} = 1.12$ [16] yield $K_H = 3.55$).

The surface charge density at the "0-plane", Q_0 (in C m^{-2}) (Fig. 3), was calculated according to the measured CEC (in meq g^{-1}) and total specific surface area of the basal surface using the following equation [16]:

$$Q_0 = -\frac{e\,N_A CEC}{10^3 SS_b}, \quad (5)$$

where e is the elementary charge (1.602×10^{-19} C) and N_A is the Avogadro number (6.022×10^{23} mol^{-1}).

The fraction of the counter-charge in the Stern layer, f_Q, is defined by:

$$f_Q = \frac{Q_\beta}{Q_\beta + Q_d}, \quad (6)$$

where Q_β and Q_d are, respectively, the surface charge densities of the Stern and diffuse layer at the basal surface (Fig. 3). The calculation of the fraction of the counter-charge in the Stern layer is very important to estimate the contributions of the Stern and diffuse layer to the complex conductivity of Na-Mt dispersions.

The interface between the basal surface and neutral water satisfies the electroneutrality condition. This implies:

$$Q_0 + Q_\beta + Q_d = 0, \quad (7)$$

ACCEPTED MANUSCRIPT

and, by combining Eqs. (6) and (7), we obtained:

$$f_Q = -\frac{Q_\beta}{Q_0}, \tag{8}$$

where Q_0 was calculated according to Eq. (5) and Q_β was computed by the modified TLM of Leroy et al. [16].

2.2.2. Water conductivity

We assume that the neutral and diffuse layer water contribute to the in-phase conductivity of the clayey materials [51-57]. The complex conductivity of the water can be described as a function of the angular frequency ω (in rad s^{-1}, $\omega = 2\pi f$ with f the frequency in Hz or s^{-1}) by considering the conduction and the displacement currents [58]. This yields:

$$\sigma_w^*(\omega) = \sigma_w + i\omega\varepsilon_w, \tag{9}$$

where σ_w is the Direct Current (DC) conductivity (in S m^{-1}) and ε_w is the dielectric permittivity (in F m^{-1}) of water (subscript "*w*" for water), and *i* is the imaginary number ($i^2 = -1$). Water dielectric permittivity is written as $\varepsilon_w = \varepsilon_r\varepsilon_0$ where ε_r is the relative dielectric permittivity of water (79.55 for Milli-Q water at a pressure of 1 bar and temperature of 295 K, which is the average temperature of our complex conductivity measurements) and ε_0 is the dielectric permittivity of vacuum (8.854×10^{-12} F m^{-1}) [59].

The DC conductivity of the water was calculated using an arithmetic formula [60, 61]:

ACCEPTED MANUSCRIPT

$$\sigma_w = \Omega_n^w \sigma_n^w + \Omega_d^w \sigma_d^w, \tag{10}$$

where Ω_n^w, σ_n^w, and Ω_d^w, σ_d^w, are the volume fractions (dimensionless) and the volume conductivities (in S m^{-1}) of the neutral and diffuse layer water, respectively. The volume fractions are given by (Appendix A):

$$\Omega_n^w = 1 - \frac{\delta_s}{V_t}\left(\frac{1}{10^3 \rho_s} + SS_o 2\chi_d\right), \tag{11}$$

$$\Omega_d^w = \frac{\delta_s}{V_t} SS_o 2\chi_d, \tag{12}$$

where δ_s is the solid mass (in g), V_t is the total volume of the dispersion (in m^3), ρ_s is the volumetric mass density of a TOT layer (in kg m^{-3}), SS_o is the outer specific surface area of the Na-Mt particles (in m^2 g^{-1} of solid, $SS_o \cong SS_b^o$), and $2\chi_d$ is the assumed thickness of the diffuse layer (in m) [45]. The parameter χ_d is the Debye length, which was calculated as a function of the water chemical composition using:

$$\chi_d = \sqrt{\frac{\varepsilon_w k_B T}{e^2 10^3 \, \mathrm{N_A} \sum_{i=1}^{N} z_i^2 C_i^w}}, \tag{13}$$

where k_B is the Boltzmann constant (1.381×10^{-23} J K^{-1}), T is the temperature (in K), N is the number of the different ionic species, z_i is the ion valence, and C_i^w is the ion concentration (in M) in the neutral water. In Eq. (13), the water chemical composition was calculated according to the known concentrations of added NaCl and HCl electrolyte and the concentrations of ions released from the contact of Na-Mt with water (Eqs. (B1)–(B4)).

ACCEPTED MANUSCRIPT

Ions in neutral water electromigrate under the applied sinusoidal electric field as long as the frequency is sufficiently low (<GHz [62]). The conductivity of the neutral water, σ_n^w, was calculated as a function of the water chemical composition using [63]:

$$\sigma_n^w = e10^3 \, \mathrm{N_A} \sum_{i=1}^{N} z_i \beta_i^w C_i^w , \quad (14)$$

where β_i^w is the mobility (in $m^2 \, s^{-1} \, V^{-1}$) of ion *i* in neutral water, which was corrected to the temperature *T* of the complex conductivity measurements using [64]:

$$\beta_i^w(T) = \beta_i^w(T_0)\left[1 + \vartheta_w (T - T_0)\right], \quad (15)$$

where $T_0 = 298\,\mathrm{K}$ and $\vartheta_w \cong 0.0227 \ \mathrm{K^{-1}}$ (considering the difference of water viscosity at *T* and T_0 [59, 65, 66]). The ion mobility at T_0 was calculated using the Nernst-Einstein equation $\beta_i^w(T_0) = (ez_i / k_B T_0) D_i^w(T_0)$ and the measured self-diffusion coefficient of ion *i* at T_0 in diluted water, $D_i^w(T_0)$ (in $m^2 \, s^{-1}$), reported in the phreeqc.dat database [65]. The ion mobilities in neutral water used in our conductivity model were reported in Table 1.

Table 1. Ion mobilities in neutral water.

Ion	β_i^w (10^{-8} $m^2 \, s^{-1} \, V^{-1}$)	
	T = 298 K	*T* = 295 K
Na^+	5.18	4.83
Cl^-	7.90	7.37
H^+	36.25	33.81
OH^-	20.52	19.14
Mg^{2+}	2.75	2.56
$H_3SiO_4^-$	4.28	3.99
SO_4^{2-}	4.17	3.89

ACCEPTED MANUSCRIPT

The volume conductivity of the diffuse layer was written as [16, 51, 53]:

$$\sigma_d^w = e10^3 \, \mathrm{N_A} \sum_{i=1}^{N} z_i B_i^d C_i^w \exp\left(-\frac{q_i \varphi_m}{k_B T}\right), \tag{16}$$

where B_d is the effective mobility of the ions in the diffuse layer (in m^2 s^{-1} V^{-1}), $q_i = \pm e z_i$ is the ion charge (in C) where "+" and "–" stand for cations and anions, respectively, and φ_m is the average electrical potential in the diffuse layer of the dispersion (in V). The potential φ_m was calculated as a function of the water chemical composition and volumetric excess of charge of the diffuse layer (Eq. (C19)). The effective ion mobility in the diffuse layer was calculated according to [16]:

$$B_i^d = \beta_i^d \pm \beta_{eo}^d \cong \beta_i^w \pm \beta_{eo}^d, \tag{17}$$

$$\beta_{eo}^d = \frac{\varepsilon_w}{\eta_w}(\varphi_m - \varphi_d), \tag{18}$$

where β_i^d is the electromigration and β_{eo}^d is the electroosmotic mobility (in m^2 s^{-1} V^{-1}) of the hydrated ions in the diffuse layer [6, 67, 68]. The parameter η_w is the dynamic viscosity of water (9.548×10^{-4} Pa s at a pressure of 1 bar and temperature T of 295 K [66]) and φ_d is the electrical potential at the onset of the diffuse layer. For instance, in the case of a difference of electrical potential of 25 mV between φ_m and φ_d at T = 295 K, Eq. (18) yields $\beta_{eo}^d \cong 1.7\times10^{-8}$ m^2 s^{-1} V^{-1}, which is in the same order of magnitude than the ion mobilities due to electromigration (Table 1).

ACCEPTED MANUSCRIPT

2.2.3. Conductivity of the Na-Mt aggregates

We consider that the polarization of the Stern layer controls the imaginary conductivity of the dispersion because most of the counter-charge is located in the Stern layer [3, 15-18, 51] and the volume of neutral water necessary for the full polarization of the diffuse layer is limited by the large volume of diffuse layer [51-55]. We assume that the diffuse layer affects the polarization of the Stern layer. Indeed, the diffuse layer must polarize to compensate the polarization of the Stern layer in order to ensure electroneutrality of the clay/water interface. We follow the work of Lyklema et al. [69] who described the effect of the diffuse layer on the Stern layer polarization. In their model, the diffuse layer decreases the relaxation time of the polarized Stern layer (Fig. 4).

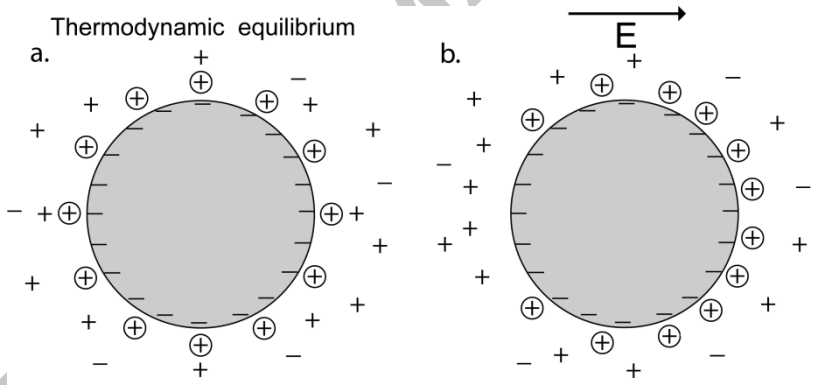

Fig. 4. Sketch of the electrochemical polarization of the Stern and diffuse layer around a spherical particle according to the polarization model of Lyklema et al. [69]. (a.) The EDL is in thermodynamic equilibrium in the absence of applied electrical field. (b.) Under the influence of the sinusoidal electrical field, as long as its frequency is sufficiently low, counter-ions and co-ions electromigrate in the Stern and diffuse layer along the particle surface. Counter-ions in the diffuse layer shorten the pathway of the counter-ions in the Stern layer to ensure the overall electroneutrality of the solid/water interface. Counter-ions and co-ions diffuse back to try to reach their initial

ACCEPTED MANUSCRIPT

concentration at thermodynamic equilibrium. A relaxation time is associated with the polarization of the Stern layer [70].

We consider the polarization of spherical and very porous Na-Mt aggregates of different sizes whose surface area is considerably increased by the external surface area of the Na-Mt particles. We do not consider the polarization of the Na-Mt particles separately. Describing the conduction and polarization a Na-Mt particle is very challenging because the shape of a Na-Mt particle is very elongated (aspect ratio between 10 and 100 [10]) and its diffuse layer is thick. For these reasons, the partial differential equations describing the complex conductivity of a Na-Mt particle (such as the Navier-Stokes and Poisson-Nernst-Planck equations [71]) must be solved numerically and cannot be easily combined with a code inverting the shape of conductivity spectra. In addition, the quadrature conductivity response of a Na-Mt particle may only occur in the kHz frequency range, and quadrature conductivity measurements in the lower frequency range may only be explained by considering the polarization of Na-Mt particles in contact with each other.

The model of Lyklema et al. [69] gives a single Debye-type conductivity response for one aggregate, which, convoluted by the aggregate size distribution, gives a generalized Debye-type conductivity response [72]. This conductivity response can be directly compared to the conductivity response inferred from the Debye decomposition approach that was used to invert the complex conductivity spectra (this will be explained in more detail in section 2.2.5).

ACCEPTED MANUSCRIPT

The complex conductivity of the aggregates can be described as a function of the angular frequency considering the conduction and the displacement currents. This implies:

$$\sigma_s^*(\omega) = \sigma_s(\omega) + i\omega\varepsilon_s, \tag{19}$$

where σ_s is the surface conductivity and ε_s is the dielectric permittivity of the aggregates (subscript "*s*" for surface), which can be calculated as a function of the volumetric mass density ρ_s using $\varepsilon_s \cong \alpha\rho_s\varepsilon_0$. The empirical parameter $\alpha = 0.00191$ $m^3\ kg^{-1}$ can be used in absence of conducting materials, such as magnetic or metallic minerals, and Fe Ti sulfides oxides such as ilmenite [73]. Robinson [74] reported $\varepsilon_s \cong 5.5\varepsilon_0$ for Mt using time domain reflectometry.

The surface conductivity of the aggregates was computed according to (Appendix D):

$$\sigma_s(\omega) = \frac{2}{3}\Omega_w\beta_S f_Q Q_V \sum_{k=1}^{L} f(d_k)\frac{i\omega\tau_k}{1+i\omega\tau_k}, \tag{20}$$

where Ω_w is the porosity, β_S is the mobility of the counter-ions in the Stern layer (in $m^2\ s^{-1}\ V^{-1}$), Q_V is the excess of charge per water volume (in C m^{-3}), and *L* is the number of effective diameters d_k (in m) of the Na-Mt aggregates. The parameter $f(d_k)$ is the discretized aggregate size distribution and τ_k is the relaxation time of the polarized Stern layer (in s). In Eq. (20), the porosity Ω_w was calculated from (Appendix C):

$$\Omega_w = \frac{\rho_s(1-w_D)}{w_D\rho_w + \rho_s(1-w_D)}, \tag{21}$$

ACCEPTED MANUSCRIPT

where w_D is the weight fraction of the dispersion and ρ_w is the volumetric mass density of water (1000 kg m^{-3} for Milli-Q water at a temperature of 298 K and pressure of one bar).

The surface mobility of Na^+ in the Stern layer (Eq. (20)) was calculated from its diffusion coefficient D_S (in m^2 s^{-1}) computed by molecular dynamics (MD) simulations (carried out at a temperature T_0 of 298 K [17, 18]). We obtained $\beta^S_{Na^+}(T_0) = 2.6\times10^{-8}$ m^2 s^{-1} V^{-1} by considering that the diffusion coefficient of Na^+ in the Stern layer is half its value in neutral water. The diffusion coefficient was converted to the surface mobility according to the Nernst-Einstein equation. The surface mobility was also corrected to the temperature *T* of the complex conductivity measurements using [64]:

$$\beta_S(T) = \beta_S(T_0)\left[1 + \vartheta_S(T - T_0)\right], \tag{22}$$

where $\vartheta_S \cong 0.04\,K^{-1}$ according to surface conductivity data inferred from electrical conductivity measurements on shaly sandstones and bentonite suspensions [64]. We obtained $\beta^S_{Na^+} = 2.2\times10^{-8}$ m^2 s^{-1} V^{-1} for *T* = 295 K.

In Eq. (20), the volumetric excess of charge was described by (Appendix C):

$$Q_V = -\rho_s\left(\frac{1-\Omega_w}{\Omega_w}\right)10^3 SS_o Q_0 . \tag{23}$$

The discretized ASD (Eq. (20)) is normalized to unity, hence:

$$\sum_{k=1}^{L} f(d_k) = 1. \tag{24}$$

The relaxation time τ_k (Eq. (20)) was written as [75]:

ACCEPTED MANUSCRIPT

$$\tau_k = \frac{1}{2\pi f_k} = \frac{{d_k}^2}{8D_S M} = \frac{{d_k}^2 |q|}{8k_B T \beta_S M}, \tag{25}$$

$$M = 1 + \frac{qQ_\beta}{k_B T C_d}, \tag{26}$$

$$C_d = -\frac{\partial Q_d}{\partial \varphi_d} = \sqrt{\frac{\varepsilon_w}{2k_B T}} \frac{\sum_{i=1}^{N} q_i 1000\,\mathrm{N_A}\, C_i^w \exp\left(-\frac{q_i \varphi_d}{k_B T}\right)}{\sqrt{\sum_{i=1}^{N} 1000\,\mathrm{N_A}\, C_i^w \left[\exp\left(-\frac{q_i \varphi_d}{k_B T}\right) - 1\right]}}, \tag{27}$$

where f_k is the relaxation frequency of the polarized Stern layer (in Hz), M (dimensionless) is a parameter characterizing the effect of the diffuse layer on the Stern layer polarization ($M \geq 1$) (Fig. 4), and q (in C) is the charge of the counter-ions in the Stern layer. The parameter q is written as $q = \pm ez$ where z is the average valence of the counter-ions, and "+" or "–" stand for cations or anions in majority in the Stern layer, respectively. The M parameter was computed using the modified TLM of Leroy et al. [16].

2.2.4. Conductivity of the Na-Mt dispersions

Following Vinegar and Waxman [57], we consider that the complex conductivity of the dispersions is the sum of the complex conductivity of the water and of the aggregates. We can make this assumption because the M-W polarization can be neglected for our SIP experiments. This implies:

$$\sigma^*(\omega) = \sigma_w^*(\omega) + \sigma_s^*(\omega). \tag{28}$$

ACCEPTED MANUSCRIPT

By combining Eqs. (9), (19), (20), and (28), we obtained for the complex conductivity of the dispersions:

$$\sigma^*(\omega) = \sigma_w + \frac{2}{3}\Omega_w \beta_S f_Q Q_V \sum_{k=1}^{L} f(d_k) \frac{i\omega\tau_k}{1+i\omega\tau_k} + i\omega(\varepsilon_s + \varepsilon_w). \quad (29)$$

The last term of Eq. (29) can be neglected because of the low-frequency range of the complex conductivity measurements (from 0.1 Hz to 45 kHz). It results that Eq. (29) can be rewritten in the form of a generalized Debye model, which describes the complex conductivity σ^* by a superposition of elementary Debye polarization terms [72, 76-78]:

$$\sigma^*(\omega) = \sigma_\infty + (\sigma_0 - \sigma_\infty)\sum_{k=1}^{L} \frac{f(d_k)}{1+i\omega\tau_k}, \quad (30)$$

$$\sigma_0 = \sigma_w, \quad (31)$$

$$\sigma_\infty = \sigma_w + \frac{2}{3}\Omega_w \beta_S f_Q Q_V, \quad (32)$$

with σ_0 and σ_∞ being the low and high-frequency limit of the in-phase conductivity, respectively. In Eq. (31), neutral and diffuse layer water contribute to the low-frequency limit of the in-phase conductivity while water and Stern layer contribute to the high-frequency limit of the in-phase conductivity (Eq. (32)).

The complex conductivity spectra were inverted using the Debye decomposition approach and the following equation to obtain the aggregate size distribution in Eq. (30) [76, 77]:

$$\sigma^*(\omega) = \sigma_\infty \left(1 - \sum_{k=1}^{L} \frac{m_k}{1+i\omega\tau_k}\right), \quad (33)$$

ACCEPTED MANUSCRIPT

with m_k being the *k*-th chargeability (dimensionless), which is a measure of the relative strength of this polarization term (weight factor). The relaxation time τ_k is inversely correlated to the frequency maximum of the quadrature conductivity of the *k*-th polarization term. Relaxation times are evenly distributed in the relaxation time range defined by the minimal and maximal data frequencies, extended by two orders of magnitude to either side.

The inversion algorithm produces relative weights $m_k(\tau_k)$ for all relaxation times τ_k, which form the relaxation time distribution (RTD). Integral, summarizing parameters can be derived from the RTD. These integral parameters summarize certain spectral features of the conductivity spectra [78]:

- The total chargeability $m_{tot} = \sum_{k=1}^{L} m_k$ accounts for the polarization magnitude in the measured frequency range.
- The normalized total chargeability $m_{tot}^n = \sigma_0 m_{tot}$ is commonly considered as a more appropriate measure of the strength of the polarization compared to the total chargeability [77, 79].
- The median relaxation time τ_{50} is the relaxation time at which 50% of the total chargeability is reached.
- The mean relaxation time τ_{mean} is the chargeability-weighted logarithmic mean value of the RTD: $\tau_{mean} = \exp(\sum_{k=1}^{L} m_k \log(\tau_k) / \sum_{k=1}^{L} m_k)$.

One important advantage of the DD scheme over more traditional phenomenological models such as the Cole-Cole model [80] is that it can describe a wide variety of different shapes of the quadrature conductivity spectra without any manual tuning (such as the need to predetermine the number of polarization peaks before fitting). Also, in

ACCEPTED MANUSCRIPT

case no polarization peaks are present in the measured complex conductivity spectra, characteristic changes can still be detected using the integral parameters mentioned before.

According to Eqs. (30)–(33), the discretized ASD was expressed as a function of the inverted chargeability distribution. We obtained:

$$f(d_k) = \frac{m_k}{\sum_{k=1}^{L} m_k} = \frac{m_k}{m_{tot}}, \tag{34}$$

where $d_k = \sqrt{8 D_S M \tau_k}$ according to Eq. (25) and $m_{tot} = (\sigma_\infty - \sigma_0)/\sigma_\infty$ [81]. Therefore, two parameters, the diffusion coefficient of the counter-ions in the Stern layer, D_S, and the effect of the diffuse layer on the Stern layer polarization, *M*, must be known to convert relaxation time distributions into aggregate size distributions.

3. Materials and methods

3.1. Properties of Kunipia-F montmorillonite

The Na-Mt dispersions were prepared using Kunipia-F (Kunimine Industries Co., Ltd, Japan), which is a sodium montmorillonite containing 95 weight per cent (wt%) of montmorillonite [82] (the remaining 5 wt% is made of silica materials). Kunipia-F contains traces of gypsum that may release sulfates in water [83]. $Na_{0.86}Ca_{0.06}Mg_{0.014}[Al_{3.14}Fe^{3+}_{0.20}Fe^{2+}_{0.04}Mg_{0.62}]^{VI}[Si_{7.80}Al_{0.20}]^{IV}O_{20}(OH)_4$ is the chemical formula of Kunipia-F [84]. Its CEC, determined by the hexamminecobalt chloride method, is 1.15 meq g^{-1} with the following initial distribution of exchangeable cations: Na 91%, Ca 8%, K 1% [84, 85]. The measured volumetric mass density of dry Kunipia particles is 2710 kg m^{-3} [85].

ACCEPTED MANUSCRIPT

3.2. Preparation of the Na-Mt dispersions

Raw Kunipia-F powders were dispersed in Milli-Q water under vigorous mechanical agitation and sonication for 3 min at 25 kHz. The clay fraction of Kunipia-F (size <2 µm) was collected by wet gravity sedimentation applying the Stokes' law on a diluted suspension with volume concentration of 0.4%. The suspension was then allowed to stand and the discharging of the fraction <2 µm was made to a height and duration determined by Stokes' law for an equivalent spherical diameter. Filtered Kunipia-F dispersions were oven-dried during two hours at a temperature of 200°C to obtain Na-Mt powders. Such high temperature was chosen to dehydrate completely Na-Mt without dehydroxylating it [86]. Different amounts of Na-Mt powders were mixed with Milli-Q water to obtain Na-Mt dispersions of weight fractions 0.5 to 5.2%. The measured pH of the Na-Mt dispersions was 10.2 ± 0.2. The pH of water in contact with Na-Mt is basic because of the sorption of the H^+ ion on the surface of Mt [13, 87, 88]. The pH of the 1% Na-Mt dispersions was adjusted to 7.3 ± 0.4 and 5.5 ± 0.4 by adding acid (HCl). The salinity of the 1% and 1.5% Na-Mt dispersions was also increased by adding NaCl. We obtained added NaCl concentrations of 10^{-4} to 0.05 mol L^{-1} (M).

3.3. Complex conductivity measurements

3.3.1. Experimental set-up

Spectral induced polarization measurements consist of imposing a sinusoidal current *I* (in A) at a given frequency (usually from 1 mHz to 10 kHz) using two current electrodes and measuring the resulting voltage *U* (in V) between two non-polarizing

ACCEPTED MANUSCRIPT

potential electrodes. According to Ohm's law, the complex impedance of the medium Z^* (in Ω) is:

$$Z^*(\omega) = \frac{U(\omega)}{I(\omega)} = |Z^*(\omega)|e^{i\phi(\omega)}, \tag{35}$$

where ϕ is the phase shift between the injected current and measured voltage (in rad). The complex conductivity $\sigma^*(\omega)$ is related to $Z^*(\omega)$ by a cell constant k (in m^{-1}), $\sigma^*(\omega) = k/[Z^*(\omega)]$. The cell constant is calculated using $k = l/S$ where l is the distance between the two potential electrodes (in m) and S is the cross-sectional area of the cylindrical sample holder (in m^2) [89, 90]. The cell constant was calculated as 273 m^{-1} considering a radius r of 1.3 cm for the cylindrical sample holder ($S = \pi r^2 \cong 5.3$ cm^2) and a distance l of 14.5 cm between the two potential electrodes.

The complex conductivity can be written as [57]:

$$\sigma^*(\omega) = \sigma'(\omega) + i\sigma''(\omega) = |\sigma(\omega)|e^{i\varphi(\omega)}, \tag{36}$$

$$\varphi = \tan^{-1}\left[\frac{\sigma''(\omega)}{\sigma'(\omega)}\right] \cong \frac{\sigma''(\omega)}{\sigma'(\omega)}, \tag{37}$$

where σ' is the in-phase conductivity, σ'' is the quadrature conductivity, and $\varphi = -\phi$ is the phase angle of the complex conductivity, i.e., the negative of the phase shift between the injected current and resulting voltage [53, 57]. The in-phase conductivity is sensitive to the conduction currents and the quadrature conductivity is sensitive to the polarization currents in the medium [53, 54]. The last approximation in the second part of Eq. (37) holds for a phase magnitude smaller than 100 mrad [53]. The phase angle $\varphi(\omega)$ defines the ratio of the polarization to the conduction currents.

ACCEPTED MANUSCRIPT

The effective conductivity, σ_{ef}, and relative dielectric permittivity, ε_{ef}, are [53, 58, 91]:

$$\sigma_{ef} = \mathrm{Re}(\sigma^*) = \sigma', \tag{38}$$

$$\varepsilon_{ef} = \frac{1}{\varepsilon_0}\mathrm{Im}\left(\frac{\sigma^*}{\omega}\right) = \frac{\sigma''}{\varepsilon_0\omega}. \tag{39}$$

SIP measurements were carried out at a temperature of 22 ± 1 °C using four brass electrodes, a sample holder and the ZEL-SIP-04 system built at Forschungszentrum Jülich GmbH including a function generator (Agilent 33120A), a measurement amplifier, an ADC card, and a PC-based measurement control system [37, 92] (Fig. 5). The length of the cylindrical sample holder made of polymethyl methacrylate (PMMA) is 30 cm, with an inner diameter of 2.6 cm. The two current electrodes are located at the top and bottom of the sample holder (electrodes 1 and 4). The two potential electrodes are located between the two current electrodes (electrodes 2 and 3) at a height of 7.75 cm and 22.25 cm from the base of the sample holder. All electrodes have a diameter of 0.6 cm and cable glands with an inner diameter of 0.7 cm are used to enable a water-tight electrode contact with the sample. The potential electrodes are retracted by 1.4 cm (twice the inner diameter of the cable gland) to avoid electrode polarization during the SIP measurements [93].

ACCEPTED MANUSCRIPT

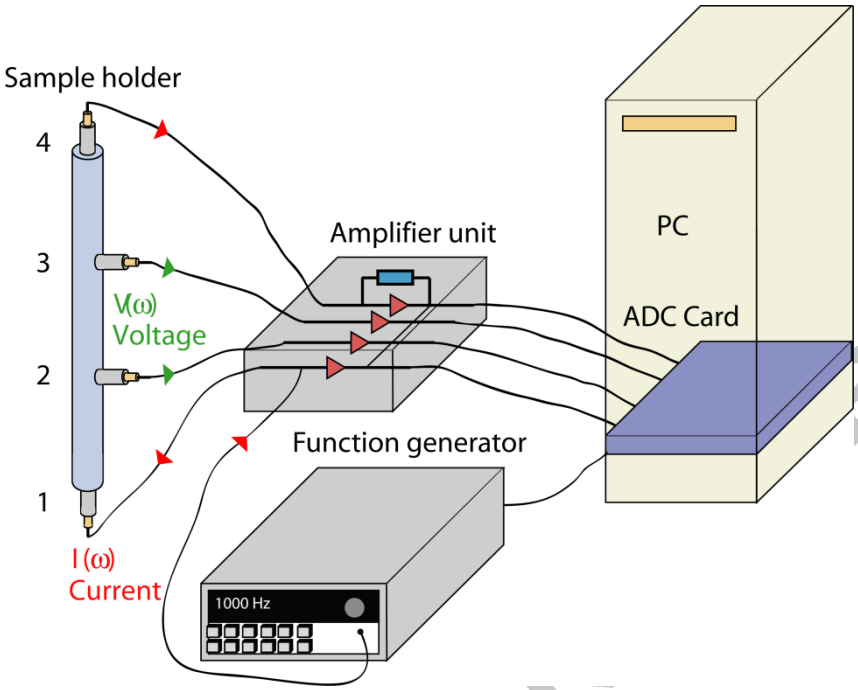

Fig. 5. Sketch of the four brass electrodes, the sample holder, and of the ZEL-SIP-04 system for spectral induced polarization measurement (modified from Zimmerman et al. [37]).

Besides the data corrections reported in Zimmerman et al. [48], measured voltages were corrected for the impedances of the potential electrodes that are known to affect measurement accuracy in the kHz range according to [94]:

$$U(\omega) = V_2(\omega)(1 + Z_{e2} i\omega C_v) - V_3(\omega)(1 + Z_{e3} i\omega C_v), \quad (40)$$

where U is the corrected voltage between the two potential electrodes (electrodes 2 and 3), $V_{2,3}$ are the measured electrical potentials at electrode 2 and 3, respectively, $Z_{e2,3}$ are the impedances of electrode 2 and 3, respectively, and C_v is the input capacitance of the amplifiers (in pF, $C_v = 4.5\,\text{pF}$ in our experiment) (Fig. 5). Impedances of the

ACCEPTED MANUSCRIPT

potential electrodes were estimated using SIP measurements with switched current and potential electrodes (i.e., reciprocal measurements) [94].

4. Comparison with experimental data

4.1. Modeling strategy and parameters values

The complex conductivity and triple layer model were written in Matlab R2013a and the Debye decomposition approach was written in the Python programming language. While the aggregate size distribution inferred from the DD approach determines the shape of the modeled complex conductivity spectra, the mechanistic complex conductivity model determines their magnitude. Fig. 6 summarizes the main features of the modeling approach. During the inversion procedure, 195 relaxation times were inverted (L = 195). The complex conductivity of the Na-Mt dispersions was computed as a function of the weight fraction of Na-Mt, the water chemical composition (Eqs. (B1)–(B4)), and the ASD inferred from the DD approach (Eqs. (25) and (34)) according to Eqs. (10)–(18), (21)–(27) and (30)–(32).

ACCEPTED MANUSCRIPT

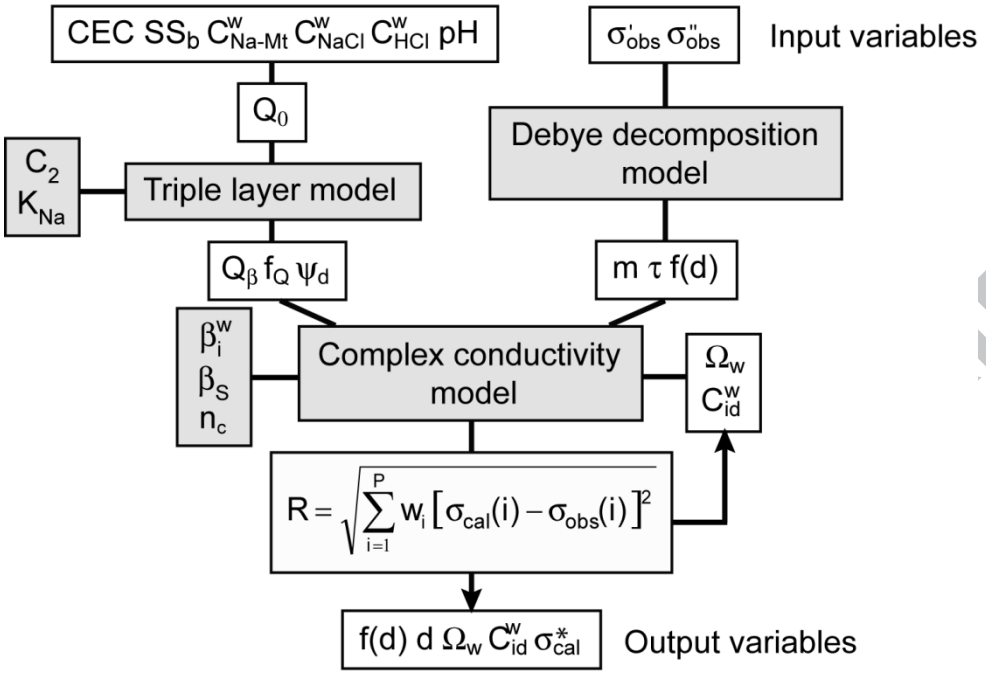

Fig. 6. Sketch summarizing the modeling strategy used to interpret complex conductivity spectra of Na-Mt dispersions (the inversion procedure used by the DD approach is not explained here, for more details, read Ref. [76]) .

The parameter values of the complex conductivity model were reported in Table 1 and Table 2. Using $CEC = 1.15$ meq g^{-1} and $SS_b = 750$ m^2 g^{-1}, we obtained for the surface charge density of the basal surface $Q_0 = -0.15$ C m^{-2}. The computed values of *M* were not sensitive to the water chemical composition and were equal to 4. This value of *M* reveals that the decrease of the relaxation time of the polarized Stern layer by the diffuse layer is significant. The computed fraction of the counter-charge in the Stern layer, $f_Q = 0.6$, shows that the majority of the counter-charge at the basal surface is located in the Stern layer. The sorption of H^+ ion in the Stern layer does not influence significantly the calculations of *M* and f_Q in the pH range 5.5 to 10.2.

ACCEPTED MANUSCRIPT

Table 2. Parameters values of the complex conductivity model.

Param.	Meaning	Value
T	Temperature of the conductivity measurements	295 K
ρ_s	Dry volumetric mass density of Kunipia Mt	2710 kg m^{-3}[a]
CEC	Cation exchange capacity	1.15 meq g^{-1}[b]
SS_b	Specific surface area of the basal surface	750 m^2 g^{-1}[c]
n_c	Number of TOT layers per Na-Mt particle	2[d]
SS_o	Outer specific surface area	375 m^2 g^{-1}[e]
Q_0	Surface charge density	–0.15 C m^{-2}[f]
M	Diffuse layer effect on Stern layer polarization	4[g]
f_Q	Fraction of the counter-charge in the Stern layer	0.6[h]
β_S	Mobility of the Na^+ ion in the Stern layer	2.2×10^{-8} m^2 s^{-1} V^{-1}[i]

[a] From Massat et al. [85].

[b] From Theng et al. [84].

[c] From Tournassat et al. [14], taking the lowest value.

[d] From Schramm and Kwak [41] who considered $n_c \in [1–2]$.

[e] Considering $SS_o \cong SS_{bo}$ and $SS_{bo} = SS_b / n_c$ (Eq. (1)) .

[f] From the reported CEC and SS_b values using Eq. (5).

[g, h] From the modified TLM of Leroy et al. [16].

[i] Calculated according to the value of $\beta^S_{Na^+}$ inferred from molecular dynamics simulations [17, 18] corrected of the temperature during the conductivity measurements (Eq. (22)).

For each SIP measurement at a given Na-Mt weight fraction and water chemical composition, the a-priori value of the porosity of the aggregates, Ω_w, was computed (Eq. (21)), and this parameter was optimized by matching the predictions of the complex conductivity model to the quadrature conductivity measurements. We also carried out lixiviation experiments on Kunipia Mt to measure the concentrations of ions released from the contact of Na-Mt with water. Results were reported in Tables A1 and

ACCEPTED MANUSCRIPT

A2 (Supporting Information file) and show that Na^+, $H_3SiO_4^-$ (dissolved SiO_2) and SO_4^{2-} ions are mostly released into water. Despite the dissolution of Na-Mt for basic pH, we consider that the Stern layer remains populated by Na^+ ions because the concentration of Na^+ ions is considerably larger than the concentrations of Mg^{2+}, Ca^{2+} or K^+ ions (Table A2). From the lixiviation experiments, we assumed a-priori that C_{id}^w = 1 mM [88, 95]. The parameter C_{id}^w was adjusted only according to in-phase conductivity measurements of basic Na-Mt dispersions (pH ≥9.3). For neutral and acid pH (pH = 7.3 and 5.5), the concentration of Cl^- ions in neutral water due to the addition of HCl, $C_{\mathrm{Cl}^- a}^w$, was also adjusted according to in-phase conductivity measurements (a-priori values were taken from the known concentrations of added HCl) (Tables A3 and A4).

As Ω_w, C_{id}^w, and $C_{\mathrm{Cl}^- a}^w$ can be adjusted independently to quadrature or in-phase conductivity measurements (C_{id}^w for basic pH, $C_{\mathrm{Cl}^- a}^w$ for neutral and acid pH), the gradient method was used to optimize these parameters. A cost function *R* between calculated and measured real or imaginary conductivity (in a least squares sense) was minimized:

$$R = \sqrt{\sum_{i=1}^{P} w_i \left[\sigma_{cal}(i) - \sigma_{obs}(i)\right]^2}\ , \tag{41}$$

where *P* is the number of frequencies investigated by each SIP measurement, w_i is a weighting coefficient (we took $w_i = 1$), and σ_{cal} and σ_{obs} are the calculated and measured real or imaginary conductivity, respectively.

ACCEPTED MANUSCRIPT

4.2. Effects of particle concentration on complex conductivity

The in-phase and quadrature conductivity, phase of the complex conductivity, effective dielectric permittivity, and computed aggregate size distributions of Na-Mt dispersions of weight fractions 0.5, 1, 1.5 and 5.2% were presented in Fig. 7. The theoretical limit of accuracy of the measured phase shift of the ZEL-SIP-04 system, 0.1 mrad, was indicated by the dotted line (Fig. 7c). The measurement uncertainties displayed by the error bars in Fig. 7 were estimated by calculating the standard deviations of the parameters using repeated conductivity measurements of the same experiment. Negative phase values, and derived quantities such as imaginary conductivity and dielectric permittivity, were omitted from the log-log plots. For frequencies below 10 Hz, only quadrature conductivity, phase and effective dielectric permittivity measurements of 1 and 5.2% dispersions were reported and show consistent trends in agreement with measurements for higher frequencies.

ACCEPTED MANUSCRIPT

ACCEPTED MANUSCRIPT

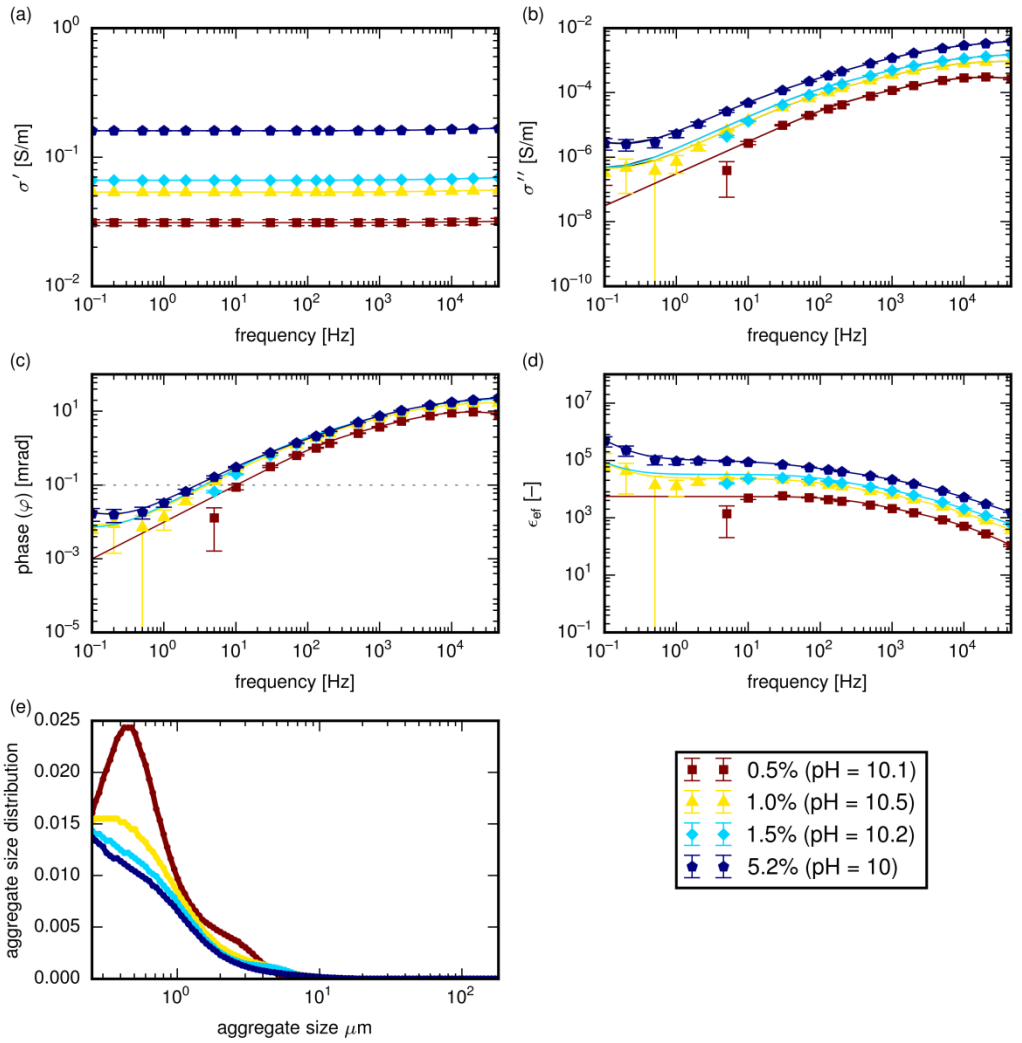

Fig. 7. In-phase conductivity (a), quadrature conductivity (b), phase (c), effective dielectric permittivity (d) as a function of frequency, and computed aggregate size distributions (e) of Na-Mt dispersions of weight fractions 0.5, 1, 1.5, and 5.2%. Symbols are experimental data and lines are the calculations from the complex conductivity model.

The quadrature conductivity increases significantly with frequency because of the polarization of more smaller Na-Mt aggregates (Figs. 7b and 7e) [22, 38]. The smaller the aggregate, the lower its relaxation time, and the higher its relaxation frequency contributing to quadrature conductivity (Eqs. (25) and (30)) [22, 51, 53]. The complex

ACCEPTED MANUSCRIPT

conductivity model reproduces very well the measurements using the aggregate size distributions presented in Fig. 7e. [22, 51, 53], which is in the range 0.3–5 μm, in agreement with centrifugal sedimentation, dynamic light scattering, and transmission electron micrograph measurements [12, 26] (Fig. 7e). ASD for sizes lower than 300 nm were not reported because they correspond to quadrature conductivity data for frequencies superior to 45 kHz interpolated by the DD approach. Aggregate size distributions also show two peaks around 400–500 and 300–400 nm for respectively 0.5% and 1% dispersions. These peaks correspond to the diameters of Na-Mt aggregates containing only a few dispersed Na-Mt particles or even to the lengths of Na-Mt particles [10, 12, 24, 26, 38, 96]. The size of the aggregate corresponding to the peak also decreases when the weight fraction increases because particles are closer together and the diffuse layer between them may be more compressed [28]. However, the peaks should be interpreted with care because they correspond to relaxation frequencies between 11.7 and 18.2 kHz (Eq. (25)). The SIP measurements above 10 kHz may have significant uncertainty (not evident from error bars in the log-log plots) due to the four-electrode set-up and the approximate correction for the contact impedances of the potential electrodes [94]. ASD also broadens when the particle concentration increases because of the polarization of more particles of different sizes and orientation [28].

In-phase, quadrature conductivity and dielectric permittivity increase quasi-linearly with the amount of particles (Figs. 7a,b,d and Fig. A1 of Supplementary Information). We explained this observation by the absence of strong electrostatic interactions between Na-Mt particles at pH = 10.2 [22] and by the increase of the surface area and volumetric excess of charge of the aggregates, whose electrochemical properties are dominated by the basal plane of surface charge density $Q_0 = -0.15$ C m^{-2} (Eqs. (C2)–(C5); Table A4). Normalized total chargeability inferred from the DD approach and describing the

ACCEPTED MANUSCRIPT

strength of the polarization, m_{tot}^{n}, also increases quasi-linearly with the amount of particles (Fig. A2 of Supplementary Information). The mean relaxation time of the dispersions (from DD) was not sensitive to their weight fraction because Na-Mt particles do not coagulate (Fig. A2) [38]. This observation also supports our assumption that the polarization of the Stern layer at the basal surface of Na-Mt may dominate the polarization of the dispersions. Indeed, one would expect that the relaxation time of the fully polarized diffuse layer (volume diffusion mechanism) decreases when the particle concentration increases [97].

Fig. 7c shows that the in-phase conductivity of 1, 1.5 and 5.2% Na-Mt dispersions is strongly related to their quadrature conductivity because the phase is not very sensitive to their weight fractions (at least for the 100 Hz to 45 kHz frequency range; $\varphi \cong \sigma''/\sigma'$, Eq. (37)) [52-55]. Only a slight increase of the phase is observed when particle concentration increases. This effect is more pronounced when the weight fraction increases from 0.5 to 1 %. This observation was explained by the conductivity of the neutral water, which may control the in-phase conductivity σ' of the 0.5% dispersions and by the Na-Mt conductivity, which may control the in-phase and quadrature conductivity of the 1 to 5.2% dispersions.

The relative dielectric permittivity, which depends on the ratio of the imaginary conductivity to the angular frequency (Eq. (39)), also increases with the particle concentration and is very high ($>10^3$) for frequencies inferior to kHz (Fig. 7d). This result suggests that the electrochemical polarization of Na-Mt dispersions occurs not only in the frequency range kHz to GHz, as previously shown by dielectric permittivity measurements with a two-electrode set-up [22, 24-26, 28, 29, 31, 32], but also in the lower Hz to kHz frequency range. Polarization in the low-frequency range may be

ACCEPTED MANUSCRIPT

expected as Na-Mt particles, even dispersed, form very porous aggregates polarizing over longer distances than individual clay particles [11, 38] (Fig. 2).

4.3. Effect of salinity on complex conductivity

When 10^{-4} to 0.06 M NaCl were added to the Na-Mt dispersions, the pH of 1% and 1.5% Na-Mt dispersions were reduced from 10.2 ± 0.2 to 10.1 ± 0.2 and to 9.8 ± 0.5, respectively. The in-phase and quadrature conductivity, phase, effective dielectric permittivity, and computed aggregate size distributions were presented in Figs. 8 and 9. Except for 1.5% dispersions containing 0.059 M added NaCl, quadrature conductivity, phase, and dielectric permittivity measurements for frequencies below 10 Hz have significant uncertainties because phases are below the accuracy limit of the ZEL-SIP-04 system (0.1 mrad).

ACCEPTED MANUSCRIPT

ACCEPTED MANUSCRIPT

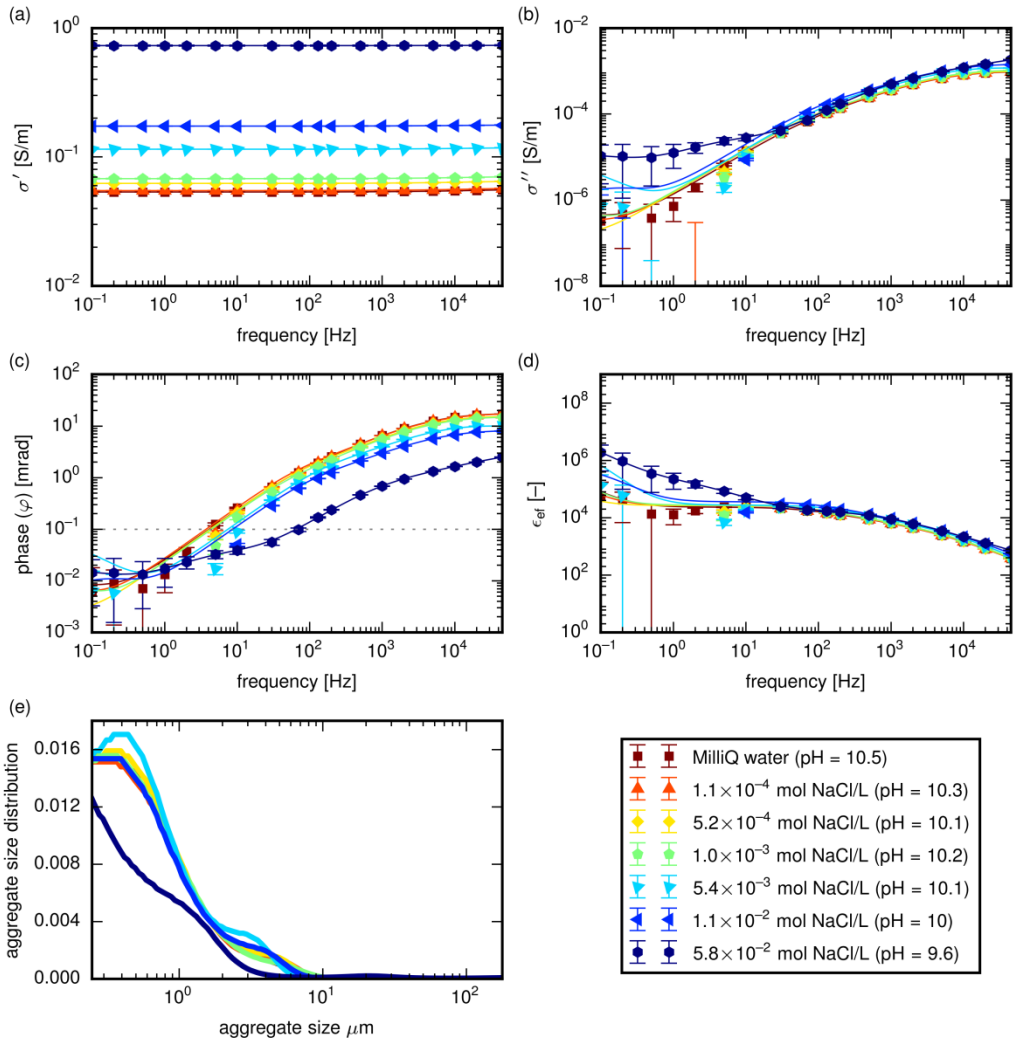

Fig. 8. In-phase conductivity (a), quadrature conductivity (b), phase (c), effective dielectric permittivity (d) as a function of frequency, and computed aggregate size distributions (e) of 1% Na-Mt dispersions at different added NaCl concentrations. Symbols are experimental data and lines are calculations from the complex conductivity model.

ACCEPTED MANUSCRIPT

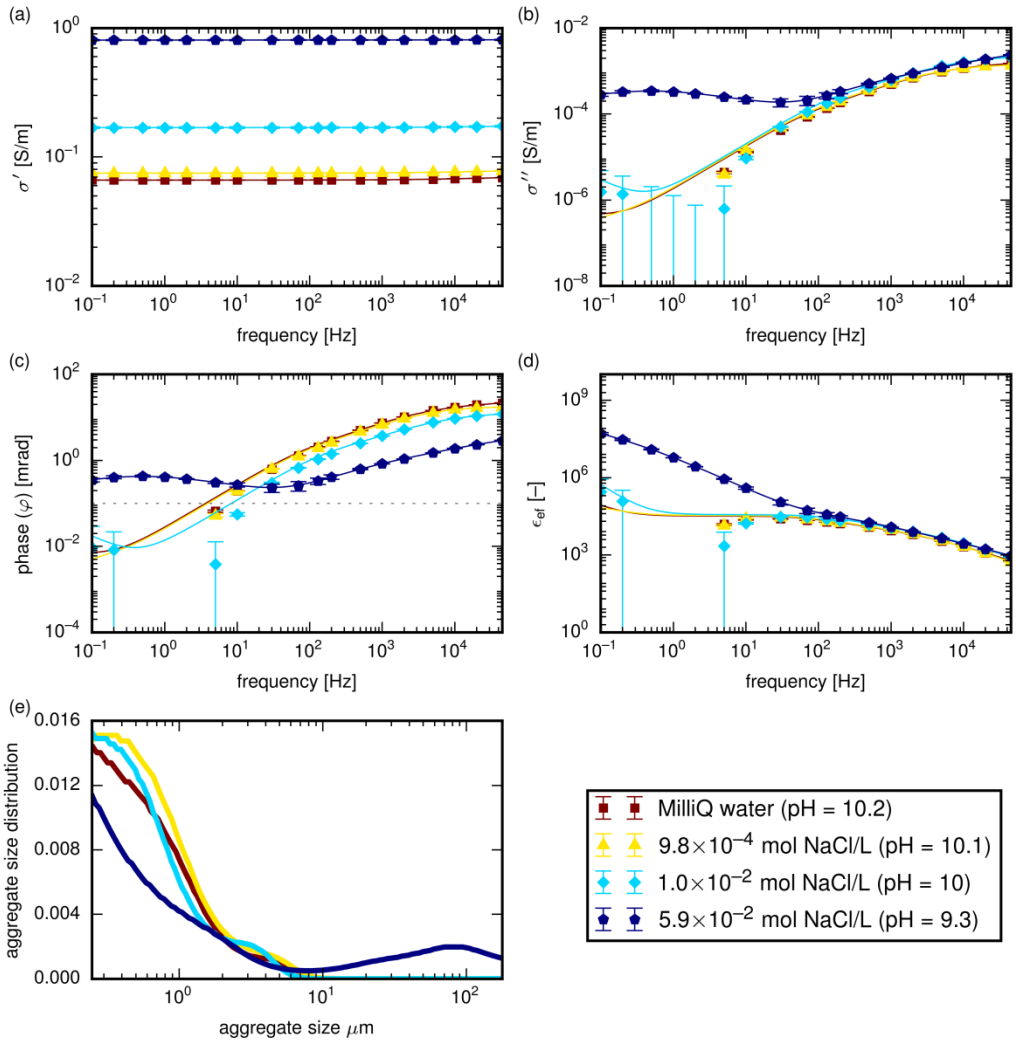

Fig. 9. In-phase conductivity (a), quadrature conductivity (b), phase (c), effective dielectric permittivity (d) as a function of frequency, and computed aggregate size distributions (e) of 1.5% Na-Mt dispersions at different added NaCl concentrations. Symbols are experimental data and lines are calculations from the complex conductivity model.

Again, the complex conductivity model describes the complex conductivity measurements very well using the aggregate size distributions presented in Fig. 8e and Fig. 9e. ASD are relatively similar when the added NaCl concentration increases up to 0.01 M NaCl. We observed less small aggregates (size inferior to one micrometer) and

ACCEPTED MANUSCRIPT

more large aggregates (size superior to ten micrometers) for 0.06 M added NaCl. A very small peak in the ASD around 20 μm and a large peak around 70-100 μm were observed for respectively 1 and 1.5% dispersions. These peaks may be due to the coagulation of Na-Mt particles into denser and considerably larger aggregates and result from the considerable increase of the measured quadrature conductivity in the low 0.1 to 100 Hz frequency range (a "peak" around 0.5 Hz is observed for σ'' of 1.5% dispersions) (Figs. 8b,e and 9b,e). The mean relaxation time of 1.5% Na-Mt dispersions (inferred from the DD approach) increases significantly when the added NaCl concentration reaches 0.06 M (Figs. A5 and A6). The modeled aggregates size in the 10–100 μm range corresponds to the size of Na-Mt aggregates in compacted Kunipia-F bentonites observed by Kozaki et al. [98] using microfocus X-Ray computerized tomography (Micro-CT) (they observed a peak around 60 μm). Coagulation of Na-Mt particles in basic water (pH = 7.5 to 8.5) has also been observed for added NaCl or $NaNO_3$ concentrations between 0.01 and 0.1 M [12, 38].

The in-phase conductivity of Na-Mt dispersions in initially Milli-Q water and in water containing around 10^{-4}, 5×10^{-4}, and 10^{-3} M added NaCl are not very sensitive to salinity (Figs. 8a and 9a) because of the conductivity of the diffuse layer and neutral water (due to ions released from Na-Mt). When the added NaCl concentration becomes higher than 10^{-3} M, the in-phase conductivity increases quasi-linearly with the NaCl concentration because the NaCl conductivity dominates the conductivity of the diffuse layer and due to released ions (Eqs. (10) and (14)) (Figs. 8a, 9a, and A4). The NaCl conductivity controls the in-phase conductivity of 1 and 1.5% Na-Mt dispersions for lower added NaCl concentrations compared to bentonite muds because of their lower solid content [53].

ACCEPTED MANUSCRIPT

The quadrature conductivity and dielectric permittivity of the dispersions are less sensitive to salinity than their in-phase conductivity and only slightly increase with salinity in the 100 Hz to 45 kHz frequency range (Figs. 8a,b,d and 9a,b,d). We explain this observation by the negative and permanent surface charge of the basal plane of Na-Mt and by the slight compression of the aggregates when salinity increases (decrease of the porosity Ω_w of the aggregates; Table A4), which may control their polarization. The increase of the compression of the diffuse layer with salinity (observed through the decreasing Debye length, Eq. (13)) and the coagulation of Na-Mt particles for the highest salinities explain the slight decrease of the porosity of the aggregates [16, 38]. The increase of the polarization of the dispersions with salinity is observed through the increase of the normalized total chargeability, which is more pronounced for 1.5% than for 1% dispersions (Fig. A5).

The phase in the 100 Hz to 45 kHz frequency range decreases when salinity increases because the in-phase conductivity increases more rapidly with salinity than the quadrature conductivity ($\varphi \cong \sigma''/\sigma'$, Figs. 8c and 9c). For frequencies below 100 Hz, the decrease of the phase with salinity slows down and the phase increases when the added NaCl concentration reaches 0.06 M because of the increase of the quadrature conductivity. In addition, like for the quadrature conductivity, the relative dielectric permittivity slightly increases with salinity for frequencies above 100 Hz (Figs. 8d and 9d). Below 100 Hz and for an added NaCl concentration around 0.06 M, the relative dielectric permittivity considerably increases when frequency decreases because it depends on the ratio of the quadrature conductivity to the frequency.

ACCEPTED MANUSCRIPT

4.4. Effect of pH and salinity on complex conductivity

The in-phase and quadrature conductivity, phase, effective dielectric permittivity and computed aggregate size distributions of 1% Na-Mt dispersions at pH = 7.3 ± 0.4 and pH = 5.5 ± 0.4 and at different added NaCl concentrations were presented in Figs. 10 and 11. The modeled aggregate size distributions have the same behavior than those obtained at pH = 10.1, with peaks in the ASD around 15 (large peak at pH = 7.3) and 35 μm (small peak at pH = 5.5). As previously observed, the in-phase conductivity is more sensitive to salinity than the quadrature conductivity and slightly increases when pH decreases from 10.1 to 7.3 and 5.5 because of the additional conductivity due to the addition of HCl (Figs. 8a, 10a and 11a).

ACCEPTED MANUSCRIPT

ACCEPTED MANUSCRIPT

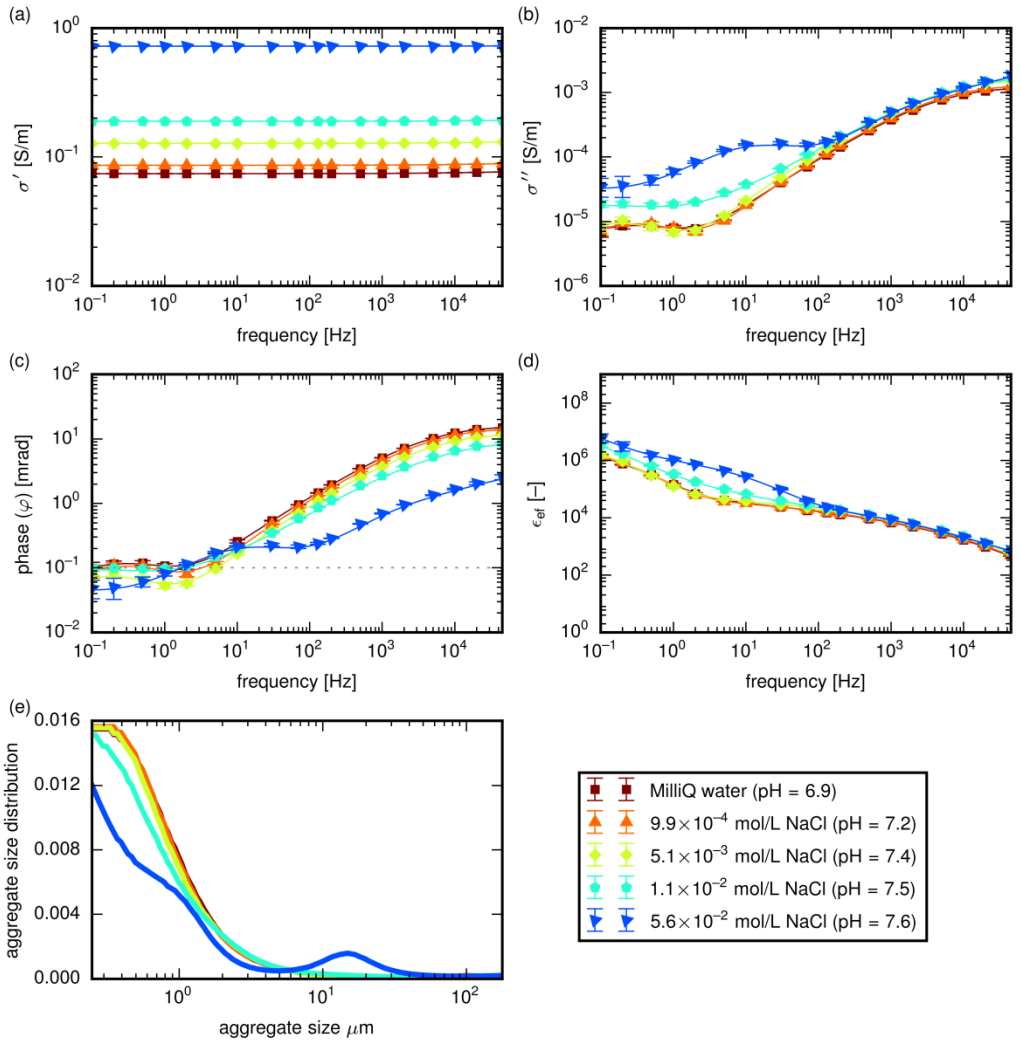

Fig. 10. In-phase conductivity (a), quadrature conductivity (b), phase (c), effective dielectric permittivity (d) as a function of frequency, and computed aggregate size distributions (e) of 1% Na-Mt dispersion at pH = 7.3 and at different added NaCl concentrations. Symbols are experimental data and lines are calculations from the complex conductivity model.

ACCEPTED MANUSCRIPT

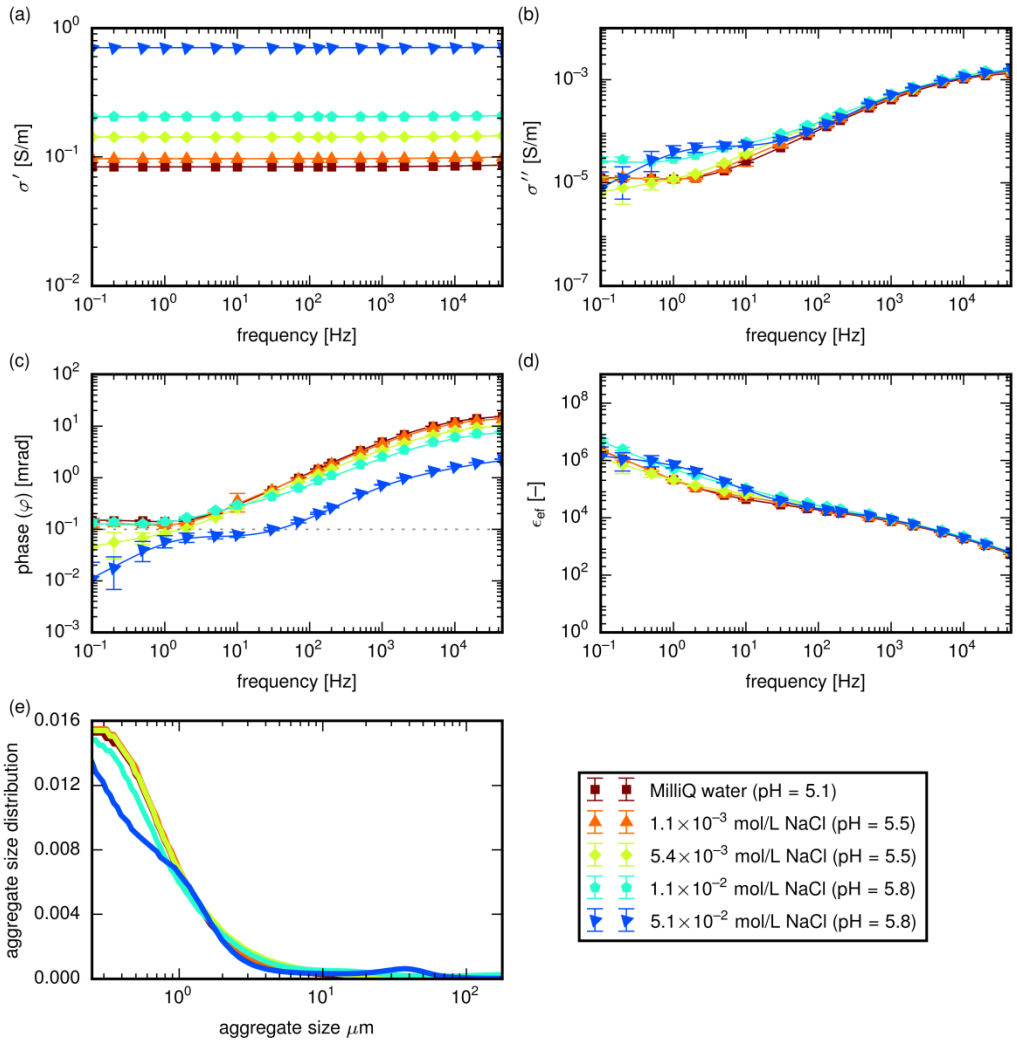

Fig. 11. In-phase conductivity (a), quadrature conductivity (b), phase (c), effective dielectric permittivity (d) as a function of frequency, and computed aggregate size distributions (e) of 1% Na-Mt dispersion at pH = 5.5 and at different added salinities (NaCl). Symbols are experimental data and lines are calculations from the complex conductivity model.

Furthermore, the quadrature conductivity in the 100 Hz to 45 kHz frequency range is relatively similar for all the pH because the electrochemical properties of the basal surface of Na-Mt, which are not very sensitive to pH, may control its quadrature conductivity (Figs. 8b, 10b and 11b and A7). Normalized total chargeability is also not

ACCEPTED MANUSCRIPT

very sensitive to pH and increases with salinity (Fig. A8). Nevertheless, the quadrature conductivity spectra in the 0.1 to 100 Hz frequency range exhibit different behaviors depending on the pH of the dispersion (Figs. 8b, 10b and 11b). The quadrature conductivity spectra at pH = 7.3 and 5.5 are relatively similar up to an added NaCl concentration of roughly 5 mM and are significantly higher than those at pH = 10.1. When the added NaCl concentration is larger than around 5 mM NaCl, the quadrature conductivity spectra at pH = 7.3 and 5.5 increase with salinity in the frequency range 0.1–100 Hz. Some "peaks" in the quadrature conductivity spectra can be observed for frequencies around 10 Hz (huge increase of the quadrature conductivity at pH = 7.3) and 2 Hz (pH = 5.5) when added NaCl concentration is around 0.05 M. The mean relaxation time of the dispersions at pH = 7.3 and pH = 5.5 is not very sensitive to the salinity and only increases significantly at pH = 7.3 for 0.056 M added NaCl (Figs. A8 and A9).

These observations can be explained by the earlier coagulation of Na-Mt particles in neutral and acid waters [12], resulting in larger modeled aggregates than for Na-Mt dispersions at pH = 10.1 (Figs. 8e, 10e and 11e). When the pH decreases from 10.1 to 7.3 and 5.5, Na-Mt particles may not be only influenced by repulsive face-to-face electrostatic interactions, but also by attractive edge-to-edge (EE) and edge-to-face (EF) interactions [12, 22, 47]. These interactions may modify the structure of the Na-Mt aggregates and the quadrature conductivity measurements in the 0.1 to 100 Hz frequency range. When the pH is neutral, Na-Mt particles have a very low edge surface charge favoring attractive EE interactions (because of van der Waals interactions) between Na-Mt particles and hence their coagulation [12, 22, 27, 99].

ACCEPTED MANUSCRIPT

5. Conclusions

The complex conductivity of Na-Mt dispersions was measured in the low 0.1 Hz to 45 kHz frequency range using a four-electrode system, the ZEL-SIP-04 apparatus. Different weight fractions of Na-Mt, from 0.5 to 5.2%, added NaCl concentrations, from 10^{-4} to 5×10^{-2} mol L^{-1}, and pH, from 5.5 to 10.2, were investigated. The measured complex conductivity spectra were inverted using the Debye decomposition approach to obtain the relaxation time and the aggregate size distributions of Na-Mt dispersions.

The complex conductivity measurements were described using a mechanistic model that considers the electrical properties of the Stern and diffuse layer at the basal surface of Na-Mt. We assume that the neutral and diffuse layer water contribute to the in-phase (real) conductivity and that the polarized Stern layer contributes to the quadrature (imaginary) conductivity of Na-Mt dispersions. The microstructural and interfacial parameters of our model were determined according to CEC, viscosity and light-transmission measurements, specific surface area estimates reported in the literature and a triple layer model of the electrochemical properties of the basal surface of Na-Mt. The concentration of ions released from the dissolution of Na-Mt in water (in the case of pH = 10) or of chloride ions due to the addition of HCl (for pH = 5.5 and pH = 7.3) were adjusted to match in-phase conductivity measurements. The porosity of the aggregates was adjusted according to quadrature conductivity measurements.

The complex conductivity measurements were successfully reproduced by our model. The modeled aggregate size distribution influences the shape and the microstructural and interfacial properties of Na-Mt the magnitude of the quadrature conductivity. The negative and permanent surface charge of the basal surface of Na-Mt may control the quadrature conductivity (or the dielectric permittivity) of the dispersions. We assume

ACCEPTED MANUSCRIPT

that 60% of the counter-charge in the EDL is located in the Stern layer and that the mobility of the Na^+ counter-ions in the Stern layer is half its value in bulk water, according to the results of recent molecular dynamics simulations. We also consider very porous aggregates (porosity ≥98%) of sizes ranging from hundreds of nanometers to tens of micrometers.

The quasi-linear increase of the in-phase and quadrature conductivity when the weight fraction of Na-Mt increases was reproduced by considering the increase of the external surface area and the volumetric excess of charge of the aggregates. The 1 and 1.5% Na-Mt dispersions also exhibit a very low surface conductivity due to their low solid content (solid volume <2%). In the 100 Hz to 45 kHz frequency range, their quadrature conductivity only slightly increases with salinity and is not sensitive to pH because it may be controlled by the surface charge of the basal surface. We explain the slight increase of the quadrature conductivity by assuming a slight decrease of the porosity and a resulting increase of the volumetric excess of charge of the aggregates. In the 0.1 to 100 Hz frequency range, the quadrature conductivity increases sharply when the added NaCl concentration is between 0.01 and 0.1 mol L^{-1} because of the possible coagulation of Na-Mt particles into larger and less porous aggregates. This phenomenon is enhanced when the weight fraction of Na-Mt increases (from 1 to 1.5%), at pH = 7.3 and in a lesser extent at pH = 5.5 because of less repulsion between Na-Mt particles.

Our work improves the understanding of the physico-chemical mechanisms controlling the conduction and polarization of Na-Mt dispersions and their electrochemical behavior. For future work, it would be very interesting to carry out aggregate size distributions measurements using different methods such as transmission electron microscopy, centrifugal sedimentation, dynamic light scattering, and coulter-counter

ACCEPTED MANUSCRIPT

measurements. It would also be very interesting to consider the full polarization of the diffuse layer to model our complex conductivity measurements.

Acknowledgments

This study was carried out within the framework of the Zetaclay and Condclay projects funded by the MIPOR program of Défi CNRS NEEDS MIPOR. The research mobility grant of P. Leroy at the Department of Earth Sciences of Uppsala University was funded by l'Institut Carnot BRGM. P. Leroy warmly thanks H. Gailhanou, M. Bizi, and S. Gaboreau for providing the Kunipia-F montmorillonite and performing filtration and lixiviation experiments. P. Leroy also thanks warmly André Revil for fruitful discussions. The authors thank the Editor and the three anonymous Reviewers for their constructing review of our paper.

ACCEPTED MANUSCRIPT

ACCEPTED MANUSCRIPT

Appendix A. Maxwell-Wagner polarization and volume fractions of the neutral and diffuse layer water

The relaxation frequency of the Maxwell-Wagner polarization of dispersions is given by [44, 100]:

$$f_{\mathrm{MW}} \approx \frac{D_w}{\pi \chi_d^{\,2}}, \tag{A1}$$

where χ_d is the Debye length and D_w is the mean diffusion coefficient of the ions in neutral water.

Eq. (A1) gives $f_{\mathrm{MW}} \geq 70$ kHz for a NaCl electrolyte at a temperature of 298 K ($D_w \cong 2\times10^{-9}\,\mathrm{m^2\ s^{-1}}$ and $\chi_d \cong 96\,\mathrm{nm}$ for an ionic strength of 10^{-5} M, Eq. (13)), which is beyond the highest frequency of our complex conductivity measurements (45 kHz). Therefore, M-W polarization can be neglected in our complex conductivity modeling.

In addition, the volume fractions of the neutral and diffuse layer water in the dispersion are defined by:

$$\Omega_n^w = V_n^w / V_t, \tag{A2}$$

$$\Omega_d^w = V_d^w / V_t, \tag{A3}$$

where V_n^w, V_d^w, and V_t are the volumes (in $\mathrm{m^3}$) of the neutral and diffuse layer water and the total volume of the dispersion, respectively. The volume of the diffuse layer is given by:

$$V_d^w = \delta_s S S_o 2\chi_d. \tag{A4}$$

The volume of the neutral water was calculated according to:

ACCEPTED MANUSCRIPT

$$V_n^w = V_t - V_s - V_d^w, \tag{A5}$$

$$V_s = \frac{\delta_s}{10^3 \rho_s}, \tag{A6}$$

and, by combining Eqs. (A4), (A5) and (A6), we obtained:

$$V_n^w = V_t - \delta_s \left(\frac{1}{10^3 \rho_s} + SS_o 2\chi_d \right). \tag{A7}$$

Finally, by combining Eqs. (A2), (A3), (A4) and (A7), we obtained:

$$\Omega_n^w = 1 - \frac{\delta_s}{V_t} \left(\frac{1}{10^3 \rho_s} + SS_o 2\chi_d \right), \tag{A8}$$

$$\Omega_d^w = \frac{\delta_s}{V_t} SS_o 2\chi_d . \tag{A9}$$

ACCEPTED MANUSCRIPT

ACCEPTED MANUSCRIPT

Appendix B. Ion concentrations in neutral water

The ion concentrations in neutral water, C_i^w, were calculated according to:

$$C_{\mathrm{Cl}^-}^w = C_{\mathrm{NaCl}}^w + C_{\mathrm{Cl}^- a}^w, \quad \text{(B1)}$$

$$C_{\mathrm{H}^+}^w \cong a_{\mathrm{H}^+}^w = 10^{-\mathrm{pH}}, \quad \text{(B2)}$$

$$C_{\mathrm{OH}^-}^w \cong K_w / C_{\mathrm{H}^+}^w, \quad \text{(B3)}$$

$$C_{\mathrm{Na}^+}^w = C_{\mathrm{Cl}^-}^w + C_{\mathrm{OH}^-}^w + C_{id}^w - C_{\mathrm{H}^+}^w, \quad \text{(B4)}$$

where C_{NaCl}^w is the concentration of added NaCl, $C_{\mathrm{Cl}^- a}^w$ is the Cl^- concentration in neutral water from HCl electrolyte, K_w is the dissociation constant of water molecules ($K_w \cong 10^{-14}$ at a pressure of one bar and a temperature of 298 K [59, 65]) and C_{id}^w is the concentration of ions released from the dissolution of Na-Mt such as $H_3SiO_4^-$, SO_4^{2-} or Mg^{2+} ions (at basic pH ≥10) [88, 95, 101].

ACCEPTED MANUSCRIPT

Appendix C. Excess of charge, porosity, and average potential of the dispersion

The excess of charge per water volume, Q_V, can be expressed as a function of the surface charge density of Mt, Q_0. These two parameters are related to each other by the overall electroneutrality condition for the dispersion, which implies:

$$\frac{1}{V_t}\left(\int_0^{V_w} Q_V dV + \int_0^{S_w} Q_0 dS\right) = 0, \tag{C1}$$

where dV, V_w, and dS, S_w, are the infinitesimal and total volume of water and infinitesimal and total external surface area (excluding the surface area of the interlayer space) of the clay, respectively.

If Q_V and Q_0 are constant, Eq. (C1) simplifies to:

$$Q_V = -\frac{S_w}{V_w} Q_0. \tag{C2}$$

The parameter S_w is given by:

$$S_w = \delta_s SS_o, \tag{C3}$$

$$S_w = \rho_s V_s 10^3 SS_o, \tag{C4}$$

$$S_w = \rho_s (1-\Omega_w) V_t 10^3 SS_o. \tag{C5}$$

The water volume is:

$$V_w = \Omega_w V_t. \tag{C6}$$

By replacing S_w and V_w in Eq. (C2) by their expressions in Eqs. (C5) and (C6), we finally obtained:

ACCEPTED MANUSCRIPT

$$Q_V = -\rho_s \left(\frac{1-\Omega_w}{\Omega_w} \right) 10^3 S S_o Q_0 . \tag{C7}$$

The relative volume of water in the dispersion was calculated as a function of its weight fraction, w_D, using:

$$\Omega_w = 1 - \frac{V_s}{V_t}, \tag{C8}$$

$$V_s = \frac{w_D \rho_w V_w}{\rho_s (1-w_D)}, \tag{C9}$$

$$V_t = V_s + V_w . \tag{C10}$$

By combining Eqs. (C8)–(C10), we obtained:

$$\Omega_w = \frac{\rho_s (1-w_D)}{w_D \rho_w + \rho_s (1-w_D)} . \tag{C11}$$

The average electrical potential in the diffuse layer of the dispersion, φ_m, was calculated according to the volumetric excess of charge of the EDL, Q_V^e, given by:

$$\frac{1}{V_t} \left(\int_0^{V_d^w} Q_V^e dV + \int_0^{S_w} Q_0 dS \right) = 0 . \tag{C12}$$

If Q_V^e and Q_0 are constant, Eq. (C12) simplifies to:

$$Q_V^e = -\frac{S_w}{V_d^w} Q_0 . \tag{C13}$$

The volume of the diffuse layer in the dispersion, V_d^w, is:

ACCEPTED MANUSCRIPT

$$V_d^w = S_w 2\chi_d \,. \tag{C14}$$

By replacing V_d^w in Eq. (C13) by its expression in Eq. (C14), we obtained:

$$Q_V^e = -\frac{Q_0}{2\chi_d} \,. \tag{C15}$$

The volumetric excess of charge of the diffuse layer is defined by:

$$Q_V^d = 1000\,\mathrm{N_A} \sum_{i=1}^{N} q_i C_i^d \,, \tag{C16}$$

$$Q_V^d = (1 - f_Q) Q_V^e \,. \tag{C17}$$

According to Eqs. (C15)–(C17), the potential φ_m was calculated by solving [15, 53]:

$$1000\,\mathrm{N_A} \sum_{i=1}^{N} q_i C_i^w \exp\left(-\frac{q_i \varphi_m}{k_B T}\right) + (1 - f_Q)\frac{Q_0}{2\chi_d} = 0 \,, \tag{C18}$$

where $C_i^d = C_i^w \exp\left(-q_i \varphi_m / k_B T\right)$.

If the compression of the aggregates is considered, Eq. (C18) becomes according to Eqs. (A3), (C5), (C7), (C13), and (C16)–(C17):

$$1000\,\mathrm{N_A} \sum_{i=1}^{N} q_i C_i^w \exp\left(-\frac{q_i \varphi_m}{k_B T}\right) + (1 - f_Q)\frac{\Omega_w}{\Omega_w^d} Q_V = 0 \,. \tag{C19}$$

ACCEPTED MANUSCRIPT

ACCEPTED MANUSCRIPT

Appendix D. Surface conductivity of a Na-Mt aggregate

We used the Schwarz's theory [70] to calculate the surface conductivity of a Na-Mt aggregate of effective diameter d_k [70]:

$$\sigma_s(\omega) = \frac{4}{d_k}\Sigma_S \frac{i\omega\tau_k}{1+i\omega\tau_k}, \quad \text{(D1)}$$

where Σ_S is the specific surface conductivity of the Stern layer (in S) [69, 75],

$$\Sigma_S = \beta_S \left|Q_\beta\right|. \quad \text{(D2)}$$

By combining Eqs. (D1) and (D2), and considering a negative surface charge Q_0 implying a positive value of Q_β, we obtained:

$$\sigma_s = \frac{4}{d_k}\beta_S Q_\beta \frac{i\omega\tau_k}{1+i\omega\tau_k}. \quad \text{(D3)}$$

Eq. (D3) cannot be directly used to describe the magnitude of the surface conductivity of a Na-Mt aggregate because its surface area is considerably higher than the surface area of a non-porous sphere. For that reason, we modified Eq. (D3) by considering the surface area ratio between the surface area of a spherical Na-Mt aggregate, S_w, and the surface area of a non-porous sphere with the same effective diameter d_k, S_k. This implies:

$$\sigma_s = \frac{4}{d_k}\beta_S Q_\beta \frac{S_w}{S_k}\frac{i\omega\tau_k}{1+i\omega\tau_k}. \quad \text{(D4)}$$

ACCEPTED MANUSCRIPT

For a non-porous aggregate, $S_w / S_k = 1$, and Eq. (D4) becomes Eq. (D3). By replacing in Eq. (D4) the parameter S_w by its expression in Eq. (C5) ($S_w = \rho_s(1-\Omega_w)V_t 10^3 SS_o$) with $V_t = \pi d_k^{\,3}/6$, and the parameter S_k by $S_k = \pi d_k^{\,2}$, we obtained:

$$\sigma_s = \frac{2}{3}\beta_S Q_\beta \rho_s (1-\Omega_w) 10^3 SS_o \frac{i\omega\tau_k}{1+i\omega\tau_k}. \tag{D5}$$

Eq. (D5) was simplified by introducing the volumetric excess of charge of the aggregate, $Q_V = -\rho_s[(1-\Omega_w)/\Omega_w]10^3 SS_o Q_0$ (Eq. (C7)). This implies:

$$\sigma_s = -\frac{2}{3}\Omega_w \beta_S \frac{Q_\beta}{Q_0} Q_V \frac{i\omega\tau_k}{1+i\omega\tau_k}. \tag{D6}$$

By introducing in Eq. (D6) the fraction of the counter-charge in the Stern layer, $f_Q = -Q_\beta / Q_0$ (Eq. (8)), we finally found for the surface conductivity of the aggregate:

$$\sigma_s = \frac{2}{3}\Omega_w \beta_S f_Q Q_V \frac{i\omega\tau_k}{1+i\omega\tau_k}. \tag{D7}$$

The surface conductivity of aggregates of different sizes was computed by convoluting the aggregate size distribution by the surface conductivity of the aggregate (superposition principle) [58, 72, 102]. We obtained:

$$\sigma_s = f(d) \otimes \sigma_s(d), \tag{D8}$$

$$\sigma_s = \sum_{k=1}^{L} f(d_k) \frac{2}{3}\Omega_w \beta_S f_Q Q_V \frac{i\omega\tau_k}{1+i\omega\tau_k}, \tag{D9}$$

$$\sigma_s = \frac{2}{3}\Omega_w \beta_S f_Q Q_V \sum_{k=1}^{L} f(d_k) \frac{i\omega\tau_k}{1+i\omega\tau_k}, \tag{D10}$$

ACCEPTED MANUSCRIPT

where $f(d_k)$ is the discretized aggregate size distribution.

ACCEPTED MANUSCRIPT

ACCEPTED MANUSCRIPT

References

[1] R.M. Garrels, F.T. Mackenzie, Evolution of sedimentary rocks, New York, 1971.
[2] L. Cary, H. Pauwels, P. Ollivier, G. Picot, P. Leroy, B. Mougin, G. Braibant, J. Labille, Evidence for TiO2 nanoparticle transfer in a hard-rock aquifer, J Contam Hydrol 179 (2015) 148-159.
[3] P. Leroy, A. Revil, A triple-layer model of the surface electrochemical properties of clay minerals, Journal of Colloid and Interface Science (2004) 371-380.
[4] D. Guisseau, P.P. Mas, D. Beaufort, J.P. Girard, A. Inoue, B. Sanjuan, S. Petit, A. Lens, A. Genter, Significance of the depth-related transition montmorillonite-beidellite in the Bouillante geothermal field (Guadeloupe, Lesser Antilles), Am Mineral 92(11-12) (2007) 1800-1813.
[5] B. Rotenberg, V. Marry, J.F. Dufreche, N. Malikova, E. Giffaut, P. Turq, Modelling water and ion diffusion in clays: A multiscale approach, Cr Chim 10(10-11) (2007) 1108-1116.
[6] M. Heuser, G. Spagnoli, P. Leroy, N. Klitzsch, H. Stanjek, Electro-osmotic flow in clays and its potential for reducing clogging in mechanical tunnel driving, B Eng Geol Environ 71(4) (2012) 721-733.
[7] M. Nouveau, G. Grandjean, P. Leroy, M. Philippe, E. Hedri, H. Boukcim, Electrical and thermal behavior of unsaturated soils: experimental results, J Appl Geophys 128 (2016) 115-122.
[8] R.E. Grim, Applied Clay Mineralogy, McGraw–Hill, New York, 1962.
[9] M. Brigatti, E. Galán, B. Theng, Chapter 2 - Structure and Mineralogy of Clay Minerals in: F.L. Bergaya, G. (Ed.), Handbook of Clay Science, Elsevier, Oxford, 2013, pp. 21-81.
[10] C. Tournassat, M. Bizi, G. Braibant, C. Crouzet, Influence of montmorillonite tactoid size on Na-Ca cation exchange reactions, Journal of Colloid and Interface Science 364(2) (2011) 443-454.
[11] M.B. McBride, P. Baveye, Diffuse double-layer models, long-range forces, and ordering in clay colloids, Soil Sci Soc Am J 66(4) (2002) 1207-1217.
[12] E. Tombacz, M. Szekeres, Colloidal behavior of aqueous montmorillonite suspensions: the specific role of pH in the presence of indifferent electrolytes, Appl Clay Sci 27(1-2) (2004) 75-94.
[13] I.C. Bourg, G. Sposito, A.C.M. Bourg, Modeling the acid-base surface chemistry of montmorillonite, Journal of Colloid and Interface Science 312(2) (2007) 297-310.
[14] C. Tournassat, C.A.J. Appelo, Modelling approaches for anion-exclusion in compacted Na-bentonite, Geochimica Et Cosmochimica Acta 75(13) (2011) 3698-3710.
[15] P. Leroy, A. Revil, S. Altmann, C. Tournassat, Modeling the composition of the pore water in a clay-rock geological formation (Callovo-Oxfordian, France), Geochimica Et Cosmochimica Acta 71(5) (2007) 1087-1097.
[16] P. Leroy, C. Tournassat, O. Bernard, N. Devau, M. Azaroual, The electrophoretic mobility of montmorillonite. Zeta potential and surface conductivity effects, Journal of Colloid and Interface Science 451 (2015) 21-39.
[17] C. Tournassat, Y. Chapron, P. Leroy, M. Bizi, F. Boulahya, Comparison of molecular dynamics simulations with triple layer and modified Gouy-Chapman models in a 0.1 M NaCl-montmorillonite system, Journal of Colloid and Interface Science 339(2) (2009) 533-541.
[18] I.C. Bourg, G. Sposito, Molecular dynamics simulations of the electrical double layer on smectite surfaces contacting concentrated mixed electrolyte (NaCl-CaCl2) solutions, Journal of Colloid and Interface Science 360(2) (2011) 701-715.
[19] C. Tournassat, J.A. Davis, C. Chiaberge, S. Grangeon, I.C. Bourg, Modeling the Acid–Base Properties of Montmorillonite Edge Surfaces, Environ Sci Technol 50 (2016) 13436-13445.
[20] M.-Y. Wu, Y. Adachi, Effects of electrolyte concentration and pH on the sedimentation rate of coagulated suspension of sodium montmorillonite, Colloids and Surfaces A: Physicochemical and Engineering Aspects 506 (2016) 686-693.
[21] J. Labille, C. Harns, J.-Y. Bottero, J. Brant, Heteroaggregation of Titanium Dioxide Nanoparticles with Natural Clay Colloids, Environ Sci Technol 49(11) (2015) 6608-6616.
[22] F.J. Arroyo, F. Carrique, M.L. Jimenez-Olivares, A.V. Delgado, Rheological and electrokinetic properties of sodium montmorillonite suspensions - II. Low-frequency dielectric dispersion, Journal of Colloid and Interface Science 229(1) (2000) 118-122.
[23] C. Grosse, A.V. Delgado, Dielectric dispersion in aqueous colloidal systems, Curr Opin Colloid In 15(3) (2010) 145-159.
[24] N.C. Lockhart, Electrical-Properties and the Surface Characteristics and Structure of Clays .1. Swelling Clays, Journal of Colloid and Interface Science 74(2) (1980) 509-519.

ACCEPTED MANUSCRIPT

[25] R. Raythatha, P.N. Sen, Dielectric-Properties of Clay Suspensions in Mhz to Ghz Range, Journal of Colloid and Interface Science 109(2) (1986) 301-309.
[26] M. Rasmusson, W. Rowlands, R.W. OBrien, R.J. Hunter, The dynamic mobility and dielectric response of sodium bentonite, Journal of Colloid and Interface Science 189(1) (1997) 92-100.
[27] A. Delgado, F. Gonzalezcaballero, J.M. Bruque, On the Zeta-Potential and Surface-Charge Density of Montmorillonite in Aqueous-Electrolyte Solutions, Journal of Colloid and Interface Science 113(1) (1986) 203-211.
[28] G. Roy, M. Pelletier, F. Thomas, C. Despas, J. Bessiere, Aggregation in Na-, K- and Ca-montmorillonite dispersions, characterized by impedance spectroscopy, Clay Miner 35(2) (2000) 335-343.
[29] L.M. Dudley, S. Bialkowski, D. Or, C. Junkermeier, Low frequency impedance behavior of montmorillonite suspensions: Polarization mechanisms in the low frequency domain, Soil Sci Soc Am J 67(2) (2003) 518-526.
[30] M. Jiménez, A. Delgado, U. Kaatze, Surface characterization of clay particles via dielectric spectroscopy, Annales UMCS, Chemistry 63(-1) (2008).
[31] Y. Tsujimoto, C. Chassagne, Y. Adachi, Dielectric and electrophoretic response of montmorillonite particles as function of ionic strength, Journal of Colloid and Interface Science 404 (2013) 72-79.
[32] Y. Tsujimoto, C. Chassagne, Y. Adachi, Comparison between the electrokinetic properties of kaolinite and montmorillonite suspensions at different volume fractions, Journal of Colloid and Interface Science 407 (2013) 109-115.
[33] M.C. Tirado, F.J. Arroyo, A.V. Delgado, C. Grosse, Measurement of the low-frequency dielectric properties of colloidal suspensions: Comparison between different methods, Journal of Colloid and Interface Science 227(1) (2000) 141-146.
[34] L.S. Collet, History of induced polarization method, in: J.B. Fink, McAlister, E. O., Sternberg, B. K., Widuwilt, W. G. and Ward, S. H. (Ed.), Induced polarization: Applications and Case Histories, Society of Exploration Geophysics, Tulsa, Oklahoma, 1990.
[35] A. Weller, F.D. Borner, Measurements of spectral induced polarization for environmental purposes, Environ Geol 27(4) (1996) 329-334.
[36] Y. Luo, G. Zhang, Theory and application of spectral induced polarization, Society of Exploration Geophysicists Tulsa, 1998.
[37] E. Zimmermann, A. Kemna, J. Berwix, W. Glaas, H.M. Munch, J.A. Huisman, A high-accuracy impedance spectrometer for measuring sediments with low polarizability, Meas Sci Technol 19(10) (2008).
[38] L.J. Michot, I. Bihannic, F. Thomas, B.S. Lartiges, Y. Waldvogel, C. Caillet, J. Thieme, S.S. Funari, P. Levitz, Coagulation of Na-Montmorillonite by Inorganic Cations at Neutral pH. A Combined Transmission X-ray Microscopy, Small Angle and Wide Angle X-ray Scattering Study, Langmuir 29(10) (2013) 3500-3510.
[39] C. Tournassat, A. Neaman, F. Villieras, D. Bosbach, L. Charlet, Nanomorphology of montmorillonite particles: Estimation of the clay edge sorption site density by low-pressure gas adsorption and AFM observations, Am Mineral 88(11-12) (2003) 1989-1995.
[40] L. Le Forestier, F. Muller, F. Villieras, M. Pelletier, Textural and hydration properties of a synthetic montmorillonite compared with a natural Na-exchanged clay analogue, Appl Clay Sci 48 (2010) 18-25.
[41] L.L. Schramm, J.C.T. Kwak, Influence of Exchangeable Cation Composition on the Size and Shape of Montmorillonite Particles in Dilute Suspension, Clay Clay Miner 30(1) (1982) 40-48.
[42] G. Sposito, K.M. Holtzclaw, C. Jouany, L. Charlet, Cation Selectivity in Sodium - Calcium, Sodium - Magnesium, and Calcium - Magnesium Exchange on Wyoming Bentonite at 298-K, Soil Sci Soc Am J 47(5) (1983) 917-921.
[43] J. Lyklema, Fundamentals of Interface and Colloid Science. Volume II: Solid-Liquid Interfaces Academic Press, London, 1995.
[44] A.V. Delgado, F. Gonzalez-Caballero, R.J. Hunter, L.K. Koopal, J. Lyklema, Measurement and interpretation of electrokinetic phenomena, Journal of Colloid and Interface Science 309(2) (2007) 194-224.
[45] R.J. Hunter, Zeta Potential in Colloid Science: Principles and Applications, Academic Press, New York, 1981.
[46] D.L. Chapman, A contribution to the theory of electrocapillarity Philosophical Magazine Serie 6 25(148) (1913) 475-481.

ACCEPTED MANUSCRIPT

[47] G. Lagaly, S. Ziesmer, Colloid chemistry of clay minerals: the coagulation of montmorillonite dispersions, Advances in Colloid and Interface Science 100 (2003) 105-128.
[48] J.D.G. Duran, M.M. Ramos-Tejada, F.J. Arroyo, F. Gonzalez-Caballero, Rheological and electrokinetic properties of sodium montmorillonite suspensions - I. Rheological properties and interparticle energy of interaction, Journal of Colloid and Interface Science 229(1) (2000) 107-117.
[49] K. Norrish, The swelling of montmorillonite, Discussions of the Faraday Society 18 (1954) 120-134.
[50] E. Ferrage, C. Tournassat, E. Rinnert, B. Lanson, Influence of pH on the interlayer cationic composition and hydration state of Ca-montmorillonite: Analytical chemistry, chemical modelling and XRD profile modelling study, Geochimica Et Cosmochimica Acta 69(11) (2005) 2797-2812.
[51] P. Leroy, A. Revil, A mechanistic model for the spectral induced polarization of clay materials, J Geophys Res-Sol Ea 114(B10202) (2009) 1-21.
[52] A. Revil, Spectral induced polarization of shaly sands: Influence of the electrical double layer, Water Resources Research 48(W02517) (2012) 1-23.
[53] G. Okay, P. Leroy, A. Ghorbani, P. Cosenza, C. Camerlynck, J. Cabrera, N. Florsch, A. Revil, Spectral induced polarization of clay-sand mixtures: Experiments and modeling, Geophysics 79(6) (2014) E353-E375.
[54] A. Revil, J.D. Eppehimer, M. Skold, M. Karaoulis, L. Godinez, M. Prasad, Low-frequency complex conductivity of sandy and clayey materials, Journal of Colloid and Interface Science 398 (2013) 193-209.
[55] A. Revil, M. Skold, S.S.H.Y. Wu, Y.X. Wu, D.B. Watson, M. Karaoulis, Petrophysical properties of saprolites from the Oak Ridge Integrated Field Research Challenge site, Tennessee, Geophysics 78(1) (2013) D21-D40.
[56] M.H. Waxman, L.J.M. Smits, Electrical conductivities in oil bearing shaly sands, Society of Petroleum Engineers Journal 8 (1968) 107-122.
[57] H.J. Vinegar, M.H. Waxman, Induced Polarization of Shaly Sands, Geophysics 49(8) (1984) 1267-1287.
[58] P. Leroy, A. Revil, A. Kemna, P. Cosenza, A. Ghorbani, Complex conductivity of water-saturated packs of glass beads, Journal of Colloid and Interface Science 321(1) (2008) 103-117.
[59] D.R. Lide, CRC Handbook of Chemistry and Physics CRC Press, Boca Raton, 1990.
[60] A. Revil, Thermal conductivity of unconsolidated sediments with geophysical applications, J Geophys Res-Sol Ea 105(B7) (2000) 16749-16768.
[61] C. Clavier, G. Coates, J. Dumanoir, Theoretical and experimental bases for the dual-water model for interpretation of shaly sands, Society of Petroleum Engineers Journal 4 (1984) 153-168.
[62] A. Revil, On charge accumulation in heterogeneous porous rocks under the influence of an external electric field, Geophysics 78(4) (2013) D271-D291.
[63] P. Debye, E. Hückel, The theory of electrolytes. I. Lowering of freezing point and related phenomena, Physikalische Zeitschrift 24 (1923) 185-206.
[64] A. Revil, L.M. Cathles, S. Losh, J.A. Nunn, Electrical conductivity in shaly sands with geophysical applications, J Geophys Res-Sol Ea 103(B10) (1998) 23925-23936.
[65] D.L. Parkhurst, C.A.J. Appelo, Description of Input and Examples for PHREEQC Version 3--a Computer Program for Speciation, Batch-reaction, One-dimensional Transport, and Inverse Geochemical Calculations, in: U.S.G.S. Reston (Ed.), U.S. Geological Survey Techniques and Methods, Book 6, Modeling Techniques, Denver, 2013, p. 497.
[66] P.W. Atkins, J. de Paula, Atkin's physical chemistry 8th Edition, Oxford University Press, Oxford, United Kingdom, 2006.
[67] J.J. Bikerman, Electrokinetic equations and surface conductance. A survey of the diffuse double layer theory of colloidal solutions Transactions of the Faraday Society 35 (1940) 154-160.
[68] A. Revil, P.W.J. Glover, Theory of ionic-surface electrical conduction in porous media, Phys Rev B 55(3) (1997) 1757-1773.
[69] J. Lyklema, S.S. Dukhin, V.N. Shilov, The relaxation of the double-layer around colloidal particles and the low-frequency dielectric-dispersion. Part I. Theoretical Considerations, J Electroanal Chem 143(1-2) (1983) 1-21.
[70] G. Schwarz, A theory of the low-frequency dielectric dispersion of colloidal particles in electrolyte solution The Journal of Physical Chemistry 66 (1962) 2636-2642.

ACCEPTED MANUSCRIPT

[71] E.H.B. DeLacey, L.R. White, Dielectric response and conductivity of dilute suspensions of colloidal particles, Journal of the Chemical Society, Faraday Transactions 2 77(11) (1981) 2007.
[72] D.P. Lesmes, F.D. Morgan, Dielectric spectroscopy of sedimentary rocks, J Geophys Res-Sol Ea 106(B7) (2001) 13329-13346.
[73] G.R. Olhoeft, Electrical properties of rocks, in: W.R.J. Y. S. Touloukian, and R. F. Roy (Ed.), Physical properties of rocks and minerals, McGraw-Hill, New York, 1981, pp. 257–339.
[74] D.A. Robinson, Measurement of the solid dielectric permittivity of clay minerals and granular samples using a time domain reflectometry immersion method, Vadose Zone J 3(2) (2004) 705-713.
[75] P. Leroy, S. Li, D. Jougnot, A. Revil, Y. Wu, Modeling the evolution of complex conductivity during calcite precipitation on glass beads, Geophys J Int (2017) 1-18.
[76] M. Weigand, A. Kemna, Relationship between Cole-Cole model parameters and spectral decomposition parameters derived from SIP data, Geophys J Int 205(3) (2016) 1414-1419.
[77] M. Weigand, A. Kemna, Debye decomposition of time-lapse spectral induced polarisation data, Comput Geosci-Uk 86 (2016) 34-45.
[78] S. Nordsiek, A. Weller, A new approach to fitting induced-polarization spectra, Geophysics 73(6) (2008) F235–F245.
[79] A. Weller, S. Nordsiek, W. Debschutz, Estimating permeability of sandstone samples by nuclear magnetic resonance and spectral-induced polarization, Geophysics 75(6) (2010) E215-E226.
[80] K.S. Cole, R.H. Cole, Dispersion and absorption in dielectrics. I. Alternating current characteristics, The Journal of Chemical Physics 9 (1941) 341-351.
[81] A. Tarasov, K. Titov, On the use of the Cole-Cole equations in spectral induced polarization, Geophys J Int 195(1) (2013) 352-356.
[82] H. Sato, T. Ashida, Y. Kohara, M. Yui, N. Sasaki, Effect of Dry Density on Diffusion of Some Radionuclides in Compacted Sodium Bentonite, J Nucl Sci Technol 29(9) (1992) 873-882.
[83] M. Ochs, B. Lothenbach, H. Wanner, H. Sato, M. Yui, An integrated sorption-diffusion model for the calculation of consistent distribution and diffusion coefficients in compacted bentonite, J Contam Hydrol 47(2-4) (2001) 283-296.
[84] B.K.G. Theng, S. Hayashi, M. Soma, H. Seyama, Nuclear magnetic resonance and X-ray photoelectron spectroscopic investigation of lithium migration in montmorillonite, Clay Clay Miner 45(5) (1997) 718-723.
[85] L. Massat, O. Cuisinier, I. Bihannic, F. Claret, M. Pelletier, F. Masrouri, S. Gaboreau, Swelling pressure development and inter-aggregate porosity evolution upon hydration of a compacted swelling clay, Appl Clay Sci 124-125 (2016) 197-210.
[86] C.M. Earnest, Thermal analysis of selected illite and smectite clay minerals. Part I. Illite clay specimens, 38 (1991) 270-286.
[87] C. Tournassat, E. Ferrage, C. Poinsignon, L. Charlet, The titration of clay minerals II. Structure-based model and implications for clay reactivity, Journal of Colloid and Interface Science 273(1) (2004) 234-246.
[88] I. Sondi, V. Tomasic, N. Filipovic-Vincekovic, Release of Silicon and Aluminum from Montmorillonite Surfaces in Aqueous Systems, Croat Chem Acta 81(4) (2008) 623-629.
[89] D. Jougnot, A. Ghorbani, A. Revil, P. Leroy, P. Cosenza, Spectral induced polarization of partially saturated clay-rocks: a mechanistic approach, Geophys J Int 180(1) (2010) 210-224.
[90] W.H. Pelton, W.R. Sill, B.D. Smith, Interpretation of complex resistivity and dielectric data. Part I, Geophys Trans 29(4) (1983) 297-330.
[91] O.A.L. de Lima, M.M. Sharma, A generalized Maxwell-Wagner theory for membrane polarization in shaly sands, Geophysics 57(3) (1992) 431-440.
[92] E. Zimmermann, Phasengenaue Impedanzspektroskopie und -tomographie für geophysikalische Anwendungen, Faculty of Mathematics and Natural Sciences, Rheinische Friedrich-Wilhelms-Universität Bonn, Bonn, Germany, 2010, p. 151.
[93] E. Zimmermann, J.A. Huisman, B. Wolters, S. van Waasen, Optimal electrode design for improved phase accuracy of spectral EIT images, 6th International Symposium on Process Tomography, Cape Town, 2012, pp. 1-10.
[94] J.A. Huisman, E. Zimmermann, O. Esser, F.-H. Haegel, A. Treichel, H. Vereecken, Evaluation of a novel correction procedure to remove electrode impedance effects from broadband SIP measurements, J Appl Geophys 135 (2016) 466-473.
[95] J.S. Chen, J.H. Cushman, P.F. Low, Rheological Behavior of Na-Montmorillonite Suspensions at Low Electrolyte Concentration, Clay Clay Miner 38(1) (1990) 57-62.

ACCEPTED MANUSCRIPT

[96] K. Kim, J.H. Kim, I.J. Chung, Effect of the clay size on the dispersion morphology and emulsion stability of ABS/layered silicate nanocomposites, J Appl Polym Sci 119(3) (2011) 1287-1296.
[97] A.V. Delgado, F.J. Arroyo, F. Gonzalez-Caballero, V.N. Shilov, Y.B. Borkovskaya, The effect of the concentration of dispersed particles on the mechanisms of low-frequency dielectric dispersion (LFDD) in colloidal suspensions, Colloids and Surfaces a-Physicochemical and Engineering Aspects 140(1-3) (1998) 139-149.
[98] T. Kozaki, S. Suzuki, N. Kozai, S. Sato, H. Ohashi, Observation of microstructures of compacted bentonite by microfocus X-ray computerized tomography (micro-CT), J Nucl Sci Technol 38(8) (2001) 697-699.
[99] I. Sondi, J. Biscan, V. Pravdic, Electrokinetics of pure clay minerals revisited, Journal of Colloid and Interface Science 178(2) (1996) 514-522.
[100] V.N. Shilov, A.V. Delgado, F. Gonzalez-Caballero, C. Grosse, Thin double layer theory of the wide-frequency range dielectric dispersion of suspensions of non-conducting spherical particles including surface conductivity of the stagnant layer, Colloids and Surfaces a-Physicochemical and Engineering Aspects 192(1-3) (2001) 253-265.
[101] S. Kaufhold, R. Dohrmann, Detachment of colloidal particles from bentonites in water, Appl Clay Sci 39(1-2) (2008) 50-59.
[102] T.R. Madden, Random Networks and Mixing Laws, Geophysics 41(Na6) (1976) 1104-1125.

ACCEPTED MANUSCRIPT

ACCEPTED MANUSCRIPT

Graphical abstract

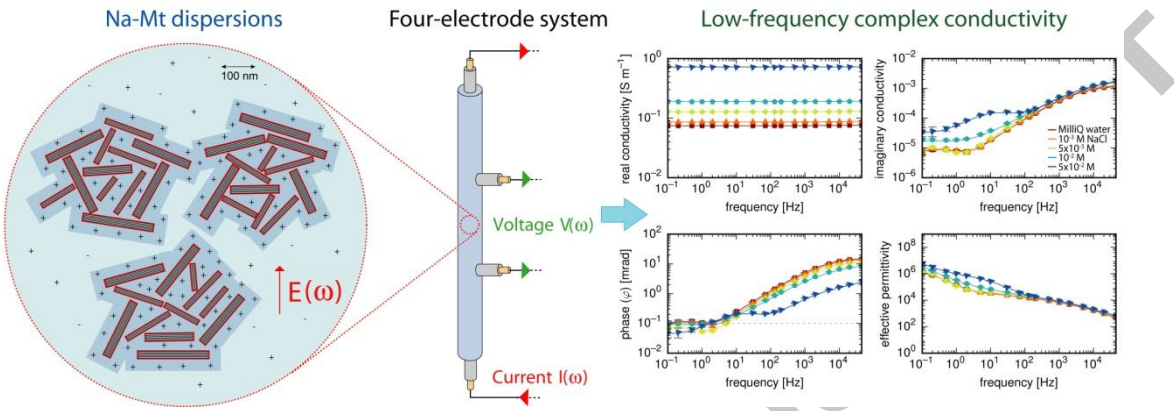

ACCEPTED MANUSCRIPT